Chemical Data Assimilation Estimates of Continental US ozone and Nitrogen budgets during INTEX-A

Pierce, R. B., T. K. Schaack, J. Al-Saadi, T. D. Fairlie, C. Kittaka, G. Lingenfelser, M. Natarajan, J. Olson, A. Soja, T. H. Zapotocny, A. Lenzen, J. Stobie, D. R. Johnson, M. Avery, G. Sachse, A. Thompson, R. Cohen, J. Dibb, J. Crawford, D. Rault, R. Martin, J. Szykman, J. Fishman

Robert B. Pierce[1] (r.b.pierce@larc.nasa.gov), Todd Schaack[2] (todds@ssec.wisc.edu), , Jassim A. Al-Saadi[3] (j.a.al-saadi@nasa.gov), T. Duncan Fairlie[1] (t.d.fairlie@larc.nasa.gov), Chieko Kittaka[1] (fn.c.kittaka@larc.nasa.gov), Gretchen Lingenfelser[1] (g.s.lingenfelser@larc.nasa.gov), Murali Natarajan[1] (m.natarajan@larc.nasa.gov), Jennifer Olson[1] (j.r.olson@larc.nasa.gov), Amber Soja[1] (a.j.soja@larc.nasa.gov), Tom Zapotocny[2] (tomz@ssec.wisc.edu), Allen Lenzen[2] (allenl@ssec.wisc.edu), James Stobie[3] (james.stobie@auatac.com), Donald Johnson[2] (donj@ssec.wisc.edu), Melody A. Avery[1] (m.a.avery@larc.nasa.gov), Glen W. Sachse[1] (g.w.sachse@larc.nasa.gov), Anne Thompson[4] (anne@met.psu.edu), Ron Cohen[5] (cohen@cchem.berkeley.edu), Jack E. Dibb[6] (jack.dibb@unh.edu), Jim Crawford[1] (j.h. crawford@larc.nasa.gov), Didier Rault[1] (d.f.rault@larc.nasa.gov), Randall Martin[7] (Randall.Martin@Dal.Ca), Jim Szykman[8] (j.j.szykman@larc.nasa.gov), Jack Fishman[1] (j.fishman@larc.nasa.gov)

1. NASA Langley Research Center, Virginia, USA
2. Space Science and Engineering Center, University of Wisconsin, Madison WI, USA
3. Science Applications International Corporation, Washington, DC, USA
4. Pennsylvania State University, University Park, PA, USA
5. University of California Berkeley, CA
6. University of New Hampshire Durham, NH, USA
7. Dalhousie University, Halifax, Nova Scotia
8. US EPA, currently at NASA Langley Research Center, Virginia, USA

Submitted to the Journal of Geophysical Research –Atmospheres (INTEX Issue)

Abstract

Global ozone analyses, based on assimilation of stratospheric profile and ozone column measurements, and NOy predictions from the Real-time Air Quality Modeling System (RAQMS) are used to estimate the ozone and NOy budget over the Continental US during the July-August 2004 Intercontinental Chemical Transport Experiment- North America (INTEX-A). Comparison with aircraft, satellite, surface, and ozonesonde measurements collected during the INTEX-A show that RAQMS captures the main features of the global and Continental US distribution of tropospheric ozone, carbon monoxide, and NOy with reasonable fidelity. Assimilation of stratospheric profile and column ozone measurements is shown to have a positive impact on the RAQMS upper tropospheric/lower stratosphere ozone analyses, particularly during the period when SAGE III limb scattering measurements were available. Eulerian ozone and NOy budgets during INTEX-A show that the majority of the Continental US export occurs in the upper troposphere/lower stratosphere poleward of the tropopause break, a consequence of convergence of tropospheric and stratospheric air in this region. Continental US photochemically produced ozone was found to be a minor component of the total ozone export, which was dominated by stratospheric ozone during INTEX-A. The unusually low photochemical ozone export is attributed to anomalously cold surface temperatures during the latter half of the INTEX-A mission, which resulted in net ozone loss during the first 2 weeks of August. Eulerian NOy budgets are shown to be very consistent with previously published estimates. The NOy export efficiency was estimated to be 24%, with NOx+PAN accounting for 54% of the total NOy export during INTEX-A.

1. Introduction

One of the key scientific goals of the 2004 phase of the Intercontinental Chemical Transport Experiment – North America (INTEX-NA) is to quantify and characterize the inflow and outflow of pollution over North America [Singh, et al. this issue]. The effects of regional air quality, over the US and elsewhere, on the global atmosphere become particularly important as world population increases require increases in agricultural production and continued economic growth leads to increased fossil fuel combustion [Stevenson et al., 2006]. Combustion leads to anthropogenic emissions of CO2, CO, NOx (NO+NO2), SO2, and non-methane hydrocarbons (NMHC) as well as particles that can significantly perturb the global atmosphere. In addition to these primary pollutants, secondary pollutants can have significant impacts on global tropospheric chemistry. In particular, the abundance and distribution of O3 governs the oxidative capacity of the troposphere. The global distribution of NOx, which is the critical limiting precursor for O3 production, is highly variable and is dependent on local photochemical loss and cycling processes involving NOx reservoir species (e.g. PAN, HNO3) as well as the magnitude of various sources which include transport from the stratosphere, natural emissions (lightning, soils, biomass burning) and anthropogenic emissions (industrial, aircraft, ships).

This study focuses on estimating ozone and NOy budgets over the Continental US and export to the global atmosphere. The approach we use is an Eulerian budget analysis as described in Pierce et al. [2003]. This analysis, which focuses on characterization of the relative contributions of 1) ozone and NOy sources and sinks within the Continental US domain and 2) regional to global exchange of ozone and NOy, should be interpreted

in light of the results from a companion manuscript by Al-Saadi et al., [this issue] which uses Lagrangian analysis techniques to characterize the influences of the global atmosphere on the chemical composition of the Continental US.

There is compelling observational and modeling evidence of the link between Continental US emissions and the global atmosphere. Knapp et al [1998] observed enhanced ozone (90-130 ppbv) just above the boundary layer over Cape Sable Island, Nova Scotia during the 1993 North Atlantic Regional Experiment (NARE). Back-trajectory analysis indicated that these air-masses had origins over the heavily industrialized N. E. United States. Model studies show episodic but significant remote influences from North America [Jacob et al., 1993; Wild et al., 1996, Atherton et al, 1996, Liang et al., 1998, Li et al. 2004], particularly in the upper troposphere. This remote influence is driven by export of NOx or PAN, which thermally decomposes to NOx [Moxim et al., 1996] and leads to further insitu ozone formation [Chameides et al., 1992]. Model based estimates of NOy export efficiency suggest that 20-30% of the NOx emitted from the Continental US is exported to the global atmosphere as NOy [Kasibhatla et al., 1993; Horowitz et al., 1998, Liang et al., 1998, Li et al., 2004]. Observational estimates of Continental US NOy export suggest efficiencies ranging from 10-15% [Parrish et al., 2004].

The preceding discussion illustrates the uncertainties that arise due to complex interactions between highly heterogeneous surface emissions, local radical chemistry, boundary layer exchange processes, enhancements in background levels of O3 and its precursors, and long range transport that ultimately determine the links between regional emissions and the global atmosphere. These links occur across multiple scales in both

time and space and therefore require a unified approach, utilizing contemporaneous satellite and insitu observations, as well as model estimates of the chemical state of the atmosphere. Field missions such as INTEX-A, which use chemical model forecast guidance to optimize synergy between insitu sampling by airborne platforms and contemporaneous satellite composition measurements for both satellite validation and science studies, are an example of this unified approach. However, an "optimized combination" of satellite, in-situ observations, and model estimates is best accomplished through chemical data assimilation. Data assimilation provides a physically consistent representation of the observed atmospheric state and involves blending information from different sources and different times to yield a best estimate, or "analysis" at a particular time. Models play an important role in data assimilation by providing an estimate, or "first guess" of the current fields based on previous analyses. The analysis is constructed by applying an "analysis increment" to the model first guess. The analysis increment is determined through variational approaches that minimize the differences between the observation and first guess under constraints that are determined by the relative errors in the respective fields [Errico, 1999].

For the current study we utilize ozone analyses (constrained with assimilated satellite measurements) and NOy predictions from the Real-time Air Quality Modeling System (RAQMS) [Pierce et al., 2003] to estimate the ozone and NOy budget over the Continental US. The manuscript is organized as follows: Section 2 provides an updated description of the RAQMS, which has undergone significant revisions since Pierce et al., [2003]. Section 3 focuses on verification of the model O3 analysis as well as CO, NOy, and O3 P-L predictions based on comparisons with satellite, ozonesonde, airborne, and

ground based measurements. Section 4 discusses the contributions to ozone and NOy in the troposphere and lower stratosphere due to stratosphere-troposphere exchange processes during INTEX-A. The Continental US ozone and NOy budgets during INTEX-A are presented in Section 5. Section 6 includes a discussion focusing on the interpretation of the INTEX-A results in light of previous studies. Section 7 provides a summary and conclusions.

1. Model Description

The chemical modeling/assimilation tool used in this study is the NASA Langley Research Center/University of Wisconsin (LaRC/UW) Real-time Air Quality Modeling System (RAQMS). RAQMS is a portable, global- to regional-scale meteorological and chemical modeling system which has been developed for assimilating remote observations of atmospheric chemical composition and predicting regional air quality within any region of the planet Earth [Pierce et al., 2003]. This study focuses on the global modeling/assimilation component of RAQMS. A companion study by Buker et al. [this issue] utilizes the regional component of RAQMS to investigate stratosphere-troposphere exchange processes over the Pacific during INTEX-A. The UW hybrid isentropic coordinate model [Schaack et al., 2004] is the dynamical core for the global component of RAQMS. Zapotocny et al. [1996, 1997a,b] established that hybrid isentropic coordinate models simulate processes involving the long-range transport of trace constituents to a higher degree of accuracy than other existing global models.

During INTEX-A RAQMS provided daily 4 day 2x2.5 degree global chemical forecasts, initialized with ozone analysis based on real-time assimilation of TOMS V8

ozone column data, to assist in flight planning. The daily assimilation/forecast cycle consisted of a series of 6 hour online chemical/dynamical forecasts, initialized with NOAA GFS meteorological analyses at 12Z, 18Z, 00Z, and 06Z. At the end of each 6hr forecast, the ozone distribution was reinitialized based on the RAQMS TOMS V8 assimilation. After 24 hours of assimilation, a 4-day online chemical/dynamical forecast was begun. For the current study, we conducted a post mission 1.4x1.4 "re-analysis" from July 01-August 15, 2004, with meteorological field initialized from the GFS analyses every 6 hours and including stratospheric ozone profile assimilation in addition to the TOMS column assimilation.

11.1 RAQMS unified stratosphere/troposphere chemistry

The RAQMS unified stratosphere/troposphere chemistry module has been developed to represent photochemical processes governing ozone formation and destruction within Earth's atmosphere from the surface to about 60 km. The chemical formulation follows a family approach with partitioning based on photochemical equilibrium approximations. Continuity equations are solved for 55 families and individual constituents and by determining equilibrium concentrations of 86 separate species. The standard Ox-HOx-NOx-ClOx-BrOx cycles governing the formation and destruction of odd oxygen, tropospheric NOx-HOx reactions, oxidation of CH4 and CO are considered [Pierce et al., 2003]. Recent updates include an extended carbon bond scheme for oxidation of non-methane hydrocarbons (NMHC) and explicit treatment of isoprene oxidation. Photochemical tendencies are calculated with a quasi-steady-state approximation based on exact solution of the continuity equation. Kinetic rates and

photolytic quantum yields and absorption cross sections are from Sander et al. [2003] with the N2+O(^{1}D) quenching rate from Ravishankara et al. [2002]. Photolytic rates are calculated using the Fastj2 method [Bian et al., 2002]. Stratospheric heterogeneous reactions on liquid aerosol [Carslaw et al., 1995] and polar stratospheric cloud [Chipperfield, 1999] surfaces are considered.

The NMHC chemical scheme is based on the lumped-structure approach of the Carbon Bond -IV mechanism (CB-IV) [Gery et al., 1989] with adjustments necessary for large-scale (regional or global) application as presented by Zaveri and Peters [1999] (henceforth called CB-Z). Additional extensions implemented in the LaRC unified chemistry include an improved isoprene oxidation scheme and the semi-explicit treatment of propane. The resulting NMHC formulation can be summarized as follows: C2H6 (ethane), C2H4 (ethene) and CH3OH oxidation are treated explicitly; C4 and larger alkanes and C3 and larger alkenes are lumped via a carbon-bond approach as updated in Zaveri and Peters [1999], with lumped groups for species such as aldehydes, ketones, peroxides and organic nitrates; C3H8 (propane) is handled semi-explicitly, i.e., C3H8 and its corresponding peroxy radicals are tracked explicitly (as in Sander et al. [2003] and Kirchner and Stockwell [1996]) while other oxidation products such as peroxides and aldehydes are lumped into the appropriate species following the carbon-bond approach for higher alkanes; and isoprene is modeled after the Carter 4-product mechanism as modified for RADM2 [Carter, 1997]. Aromatic chemistry is not included. Concentrations of 2 species, acetone and methanol, are currently specified according to climatologies.

Zaveri and Peters [1999] present smog chamber experiments showing that the CB-Z mechanism is accurate to within 5-20% error under highly polluted conditions. For the

more remote conditions encountered under regional and global scale modeling, Zaveri and Peters [1999] compared the CB-Z mechanism to that of RADM2 (Regional Acid Deposition Model-2 [Stockwell et al., 1990, 1997]) and found that CB-Z model calculations were generally within 20% of RADM2 for these multi-day rural simulations, a significant improvement with respect to the comparison of the original CB-IV with RADM2 (50-95% differences). The replacement of the CB-Z isoprene oxidation scheme with a more detailed four-product mechanism allows more accurate representation of PAN, an important nitrogen reservoir species. The four-product mechanism explicitly represents the major identified secondary isoprene oxidation products methacrolein (MACR), methyl vinyl ketone (MVK) and peroxymethacryloyl nitrate (MPAN). Rate constants, products and yields have been updated as reported in the literature (e.g., Orlando et al. [2002]).

To test the fidelity of the NMHC mechanism within the LaRC unified chemical module, point calculations using data from the GTE TRACE-P flight campaign were conducted and compared with results from the LaRC boxmodel [Crawford et al., 1999]. The LaRC boxmodel has a NMHC chemical scheme based on the condensed lumped molecule mechanism in Lurmann et al. [1986]. The two models were run to diurnal equilibrium with values of O3, CO, NMHCs, temperature, dew point and pressure constrained to observations. NO was allowed to vary diurnally, but total short-lived nitrogen (NO+NO2+NO3+2N2O5+HONO+HNO4) is held constant such that the predicted NO matched to observations at the time of measurement. Model calculations are also constrained by H2O2, CH3OOH, HNO3, PAN and acetone when measurements are available; otherwise these species are calculated.

The two models yield nearly identical results when NMHC species are neglected, thus differences using full chemistries provide a measure of uncertainties introduced by the choice of NMHC chemical scheme. Median differences between the two models when NMHC reactions are included are within 10% or less, and the LaRC unified chemistry is slightly more reactive (lower radical concentrations) compared to the Lurmann boxmodel mechanism. The one-to-one correspondence between the models is quite good, with correlation coefficients better than 0.99 for calculated OH, HO2 and CH2O.

Climatological emissions of NOx and CO include anthropogenic and natural sources and are based largely on 1x1 degree public databases available from GEIA/EDGAR with updates for Asian emissions from Streets et al. [2003] and additional biogenic CO sources as described by Duncan et al. [2004]. Aircraft NOx emissions are obtained from the HSRP database [Stolarski et al., 1995]. Lightning NOx emissions are calculated based on Price et al. [1997] using instantaneous convective cloud heights, and are distributed in the vertical according to Pickering et al. [1998]. Biomass burning emissions of NOx are scaled to those of CO. Emissions of NMHC species are generally based on the GEIA database. Surface sources of N2O, CH4, and halocarbons are implicitly assumed by imposing a constant mixing ratio at the surface appropriate for 1990 [WMO, 1993]. Surface deposition is computed according to the surface type and drag coefficients, with the calculation of the deposition rate modeled after Galbally and Roy [1980] and Levy et al. [1985]. Dry deposition is computed for O3, peroxides, aldehydes, NO2, CO and nitric acid using deposition velocities from Muller and Brasseur [1995]. Online wet removal of soluble species is based on convective fluxes and precipitation amounts [Liu et al., 2001;

Park et al., 2004]. Tropospheric heterogeneous loss of N2O5 is based on zonal averaged rates from Dentener and Crutzen [1993].

2.2 RAQMS Ecosystem based wild fire emission inventory

Alaskan and Canadian wild fires had a significant impact on North American chemical composition during INTEX-A. The RAQMS biomass burning emissions for Alaska and Canada use an ecosystem based approach developed by Soja et al [2004] to predict total direct carbon emissions. Soja et al [2004] used a spatially and temporally explicit model that incorporated a satellite-based (AVHRR) fire database and ecoregion-specific carbon consumption estimates for three classes of severity to estimate a range of total direct carbon and trace gas emissions from fires in Siberia from 1998 through 2002. We have extended this algorithm to North America using MODIS thermal anomaly data to provide area burned estimates [Soja et al., this issue]. Briefly, the approach is as follows:

(i) Static carbon consumption estimates for low-severity surface fires, medium-severity fires, and high-severity fires are based on the amount of carbon contained in individual ecosystems [Olson et al., 1983; Zinke et al., 1986].

(ii) Daily 1x1 degree North American area burned estimates are obtained using MODIS thermal anomaly products.

(iii) Based on carbon consumption and area burned, daily total direct carbon emissions from fire events in Alaska and Canada are estimated for June-August 2004 assuming all wild-fires were high-severity fires.

(iv) 1x1 degree species-specific emission estimates are determined using existing emission ratios from grassland, temperate and boreal ecosystems from across North America (Cofer et al., 1996a,b, Vose, 1996).

Assuming high-severity for all Alaskan and Yukon fires must be considered an upper bound on the actual emissions and results in the release of 70 Tg CO during the period from June-August 2004, which is a factor of 2 times higher the emissions obtained by Pfister et al. [2005] during the same period using MOPITT data to constrain inverse modeling based estimates of the Alaskan/Yukon emissions. In the future, improved emission estimates that account for changes in fire severity will be obtained using the US Forest Service Haines Index. The Haines Index is the sum of a stability term and a moisture term. The sum provides an indication of the potential for the rate of spread (ROS) of a fire on a given day.

2.3 RAQMS Chemical Data Assimilation

Data assimilation provides a statistically robust means of blending model predictions and observations to provide an optimal estimate of the true state of the atmosphere. Global assimilation of chemical measurements from polar orbiting satellites has been shown to improve estimates of the true atmospheric state [Lamarque et al., 1999; Jeuken et al., 1999, Stajner et al., 2004] and is used by RAQMS to provide an optimal estimate of the global ozone distribution during INTEX-A. RAQMS uses the statistical digital filter (SDF) analysis system [Stobie 1985, 2000] to perform a univariate assimilation of stratospheric profile and total column ozone observations. The SDF formalism is based on optimal interpolation (OI). However, rather than viewing the

analysis as a minimization problem, SDF treats the analysis as a digital filtering problem [Oppenheim and Schafer 1975]. In SDF, solving the OI equations at each grid point is equivalent to convolving a low-pass digital filter with the observation innovations (observed value minus first guess value). The spectral response of the filter is determined by the number of observations used per grid point, the observation spacing, the observation errors, the first guess and the first guess error correlation model [Stobie 2000]. Estimates of the RAQMS forecast error variances are calculated by inflating the analysis errors (a by-product of the analysis) using the error growth model of Savijarvi [1995]. The quality control employed during the analysis includes a gross check, suspect identification and a buddy check for suspect observations.

Stratospheric (tropopause and above) HALOE, SAGE II, and SAGE III solar occultation measurements, were assimilated at 6hr (00Z, 06Z, 12Z, 18Z) intervals to provide constraints on the stratospheric ozone mixing ratios. Assimilation of TOMS V8 cloud cleared total column ozone measurements were used to provide constraints on the RAQMS total column analysis. The RAQMS column assimilation accounts for the vertical variation in the retrieval sensitivity by convolving the model first guess ozone profile with the zonal mean, time averaged sensitivity and the 3D monthly apriori used in the TOMS V8 retrieval algorithm. Special SAGE III limb scattering measurements [Rault, 2005; 2006] were taken over North America and the North Atlantic during the later half of July and mid August. These measurements were also assimilated. Figure 1 shows a latitude time series of the frequency of observations used in the RAQMS assimilation. The symbols indicate the location of the solar occultation and limb scattering observations while the contours indicate the density of the cloud-cleared total

column measurements expressed as zonal mean percentages of the total available observations. During Julian days 183-197 (July 01-14, 2004) SAGE III and HALOE solar occultation measurements provide profile constraints in the Northern Hemisphere stratosphere. During Julian days 198-214 (July 15-31, 2004) SAGE III limb scattering (restricted to North America and North Atlantic sectors) and SAGE II solar occultation measurements provide additional stratospheric constraints. During Julian days 215-226 (August 01-12, 2004) there are very few stratospheric profile measurements to provide constraints for the ozone assimilation in the northern hemisphere stratosphere.

3. Model Verification

3.1 **Comparison with satellite observations**

Figure 2 shows the comparison between RAQMS and cloud cleared MOPITT CO column for the period from July01-August 15, 2004. The Continental US domain used in the budget calculations is also shown. To perform this comparison, 6 hourly RAQMS CO profiles were mapped onto MOPITT observation points and interpolated in time to the standard MOPITT retrieval levels, then the averaging kernel for each retrieval was used in conjunction with the MOPITT apriori to determine the "retrieved" RAQMS CO profile, which was integrated in the vertical using the MOPITT retrieval levels. The resulting RAQMS "retrieved" and MOPITT retrieved CO columns were binned in 1x1 degree bins. RAQMS is highly correlated with MOPITT on both regional (continental US correlation is .92) and global (correlation is .78) scales. RAQMS biases relative to MOPITT are very small (median biases of less than 0.01 $x10^{18}$ mol/cm^2, or <1%, globally

and 0.02×10^{18} mol/cm^2, or 1.2%, over the Continental US). RAQMS overestimates the CO column relative to MOPITT over Alaska and Western Canada, where the RAQMS "retrieved" column is up to a factor of 2 higher than MOPITT. This is consistent with the factor of 2 higher total wild fire emissions in the RAQMS simulation relative to the MOPITT constrained emissions used by Pfister et al., [2005]. RAQMS underestimates the CO column by 50% relative to MOPITT over central Africa. This is because climatological biomass burning emissions were used in this region. RAQMS also underestimates the CO column over S.E. Asia and the western Pacific.

Figure 3 shows the comparison between RAQMS and cloud cleared tropospheric NO2 columns retrieved from SCIAMACHY by Martin et al. [in press] for the period from July 01-August 15, 2004. In these comparisons, instantaneous RAQMS NO2 profiles were extracted from the model integrations at the SCIAMACHY observation points to account for the rapid diurnal variation in stratospheric NO2. We did not account for the airmass factor used in the SCIAMACHY tropospheric NO2 retrieval. The AMF calculation of the retrieval uses relative vertical NO2 profiles (shape factors) from GEOS-CHEM. However, little bias is expected in the comparison with RAQMS since the shape factors are determined largely by the spatial distribution of NOx emissions [Martin et al., 2002], a distribution which is similar between the two models. The resulting predicted and measured tropospheric NO2 columns were binned in 1x1 degree bins. Due to the large dynamic range of the tropospheric column NO2 measurements the log of the NO2 columns are shown. As was found with MOPITT, the RAQMS spatial distribution is strongly correlated with SCIAMACHY (global correlation of .65 and continental correlation of .64) but RAQMS tends to underestimate

tropospheric NO2 columns relative to SCIAMACHY both globally (median bias of -.33 $x10^{15}$ mol/cm^2, or 52%) and regionally (continental US median bias of -.81 $x10^{15}$ mol/cm^2, or 46%). The systematic low bias over most of the Northern Hemisphere land masses may be associated with unaccounted for soil emissions [Bertram et al., 2005; Jaegle et al., 2005]. The relatively coarse resolution of the RAQMS simulation significantly impacts the inability to accurately describe urban "hot spots", which also contributes to the median low biases.

Figure 4 shows the comparison between RAQMS and climatological (1979-2000) tropospheric ozone determined from TOMS total column and SBUV2 stratospheric measurements using residual techniques [Fishman and Balok, 1999]. To estimate the climatological July 01-August 15 mean we have used a 2/3 to 1/3 weighting of the July and August climatological means. The RAQMS 2004 tropospheric ozone analysis is generally consistent with climatological expectations both globally (correlation of .73 and median bias of 1.09 DU, or 3%) and over the continental US (correlation of .79 and median bias of 1.23DU, or 3%) except over Northern Africa and Southern Europe, where the RAQMS analysis is approximately 10-20 DU higher than climatology. This broad region of elevated tropospheric ozone column is roughly coincident with the location of the subtropical jet and tropopause break, and was significantly influenced by stratosphere-troposphere exchange processes during INTEX-A [Al-Saadi et al. this issue].

Jing et al. [2004], using contour advection of potential vorticity mapped SAGE II ozone measurements for 1990, showed enhanced (over 2 Tg/month) isentropic stratosphere to troposphere ozone transport along the 345K potential temperature surface,

which is roughly coincident with the mid-latitude tropopause. The enhanced ozone transport extended in a broad meridional band from the N.E. US, across the Central Atlantic, and over Northern Africa in a pattern that is remarkably similar to the Atlantic and European ozone enhancements found in the RAQMS ozone analysis. There is some evidence of this pattern in the TOMS-SBUV2 climatology, however, the Fishman and Balok [1999] TOMS-SBUV2 climatology only includes tropospheric ozone residuals that are less than 75 DU, which would tend to filter out influences of stratosphere to troposphere exchange processes on the climatological tropospheric ozone.

To determine whether this column ozone enhancement is real or a model artifact we compared the RAQMS ozone analysis to 8 World Meteorological Organization (WMO) ozonesondes that were launched during the period from July 08 to August 10, 2004 from Santa Cruz, Tenerife, (location shown on Figure 4). Figure 5 shows results from the statistical analysis of the WMO ozonesonde data. The observed ozone profile shows persistent ozone enhancements (mean values of 80ppbv) above 500mb. Compared to the WMO ozonesonde data, the Santa Cruz RAQMS ozone analyses shows mean high biases of 10% or less below 400mb. However, the high bias in the RAQMS analysis increases to nearly 35% at the tropopause (near 150mb), suggesting that while there is clearly upper tropospheric ozone enhancement at Santa Cruz it is overestimated in the RAQMS ozone analysis. A 35% overestimate in upper tropospheric ozone has a relatively small effect on the tropospheric ozone column. The mean observed and analyzed ozone columns below 150mb were 43.9DU and 48.4DU, respectively. The resulting 4.5DU overestimate is approximately 10% of the observed column.

3.2 Comparison with IONS ozonesonde and EPA AIRNOW networks

The INTEX Ozonesonde Network Study (IONS) [Thompson et al, this issue] provided multiple daily ozonesonde launches during INTEX-A. The unprecedented duration (July 01-Aug 14), frequency (daily), and density (up to 12 ozonesonde stations) makes this data set extremely useful for verification of the RAQMS ozone assimilation as well as science studies [Thompson et al, 2006]. Figure 6 shows composite timeseries of the IONS ozonesonde data along with comparisons with the RAQMS ozone analysis. The IONS composite was obtained by binning all the daily ozonesondes in log-pressure bins (10 bins/decade in pressure). The RAQMS composite was obtained in the same manner after mapping the RAQMS ozone analysis to the full resolution ozonesonde. Mean errors were estimated by averaging the point-by-point errors for all profiles within each pressure bin. RMS errors were estimated in the same way after removing the mean bias within each pressure level. The daily mean pressure of the thermal tropopause on the northern boundary of the Continental US budget domain, and 380K potential temperature surface on the southern boundary of the budget domain are also indicated. These surfaces define the maximum vertical extent of the middle world [Holton, 1999] over the Continental US. The middle world is a region in the lower stratosphere that is strongly coupled to the subtropical upper troposphere due to quasi-horizontal, isentropic exchange near the subtropical jet. This quasi-horizontal exchange occurs because of the sharp meridonal gradient in the tropopause altitude near the subtropical jet. The IONS composite shows significant day to day variability in this region, as evidenced by the altitude of the 250ppbv ozone mixing ratio (which is roughly coincident with the thermal tropopause) prior to mid July (Julian day 200) then there is an extended period with less variability,

followed by renewed variability during early August (Julian day 215). The RAQMS ozone analysis does a good job in reproducing this composite behavior, which is largely driven by upper tropospheric planetary wave activity.

Upper tropospheric ozone mixing ratios of 100 ppbv or more are most likely stratospherically influenced airmasses. The IONS composite shows significant variability in the frequency of stratospherically influenced tropospheric ozone measurements, defined here as composite ozone mixing ratios greater than 100 ppbv but observed below northern tropopause of the Continental US domain. In the IONS composite, signatures of stratospherically influenced ozone extend down to 500mb during the middle 3 weeks of INTEX-A. There are relatively fewer observations of stratospheric influenced air in the troposphere during the first 2 weeks of July (Julian days 183-198) and second week of August (Julian days 227-234). This is consistent with Avery et. al., [this issue] who find evidence for interleaving and mixing of stratospherically influenced and polluted tropospheric air in the vicinity of the subtropical jet for INTEX-A flights in late July and early August.

The observed variations in the depth of the stratospherically influenced air in the upper troposphere are not as pronounced in the RAQMS composite, leading to predominately positive analysis errors in the upper troposphere during the beginning and end of INTEX-A and predominately negative analysis errors in the upper troposphere during the middle of INTEX-A. The positive analysis errors at the beginning an end of the mission frequently reach 40-50% and extend down to as far as 600mb while the negative analysis errors are typically only 20-30%. During the last two weeks of July and first week of August the frequency and vertical extent of large positive analysis errors are

significantly reduced , with the majority of the analysis errors between +/- 20% during the middle part of INTEX-A.

The first part of this period of relatively low analysis errors (July 15-31) corresponds to the period when daily SAGE III limb scattering measurements, made over a wide latitude band over the Continental US, were assimilated. The reduction in the extent and frequency of significant high biases in the analysis during this period indicates that the assimilation of SAGE III limb scattering measurements had a positive impact on the RAQMS ozone analysis, particularly in the upper troposphere/lower stratosphere. The fact that these improvements persist for at least 5 days after the limb scattering assimilation stops indicates that the system has memory of the measurements, which has significant implications for air quality forecasting. The RMS analysis errors over the Continental US are largest within the middle world and are typically on the order of 40-60%, although occasionally RMS errors reach up to 80-100%. These errors are most likely associated with errors in the vertical placement of stratospheric and subtropical ozone lamina that were frequently observed during INTEX-B [Thompson et al., 2006]. There are occasional RMS errors of up to 40% near the surface, but these appear to occur during periods of relatively low boundary layer ozone events and are not likely to be significant.

Figure 7 summarizes the RAQMS/IONS comparison with a time averaged comparison between the RAQMS ozone analysis and all ozone profiles during INTEX-A. In addition to mean and rms errors we also assess the ability of the RAQMS analysis to capture the observed variability, defined here as the overall temporal and site to site variability at a given pressure level. Above 100mb, the mean analysis biases are on the

order of 10% with rms errors of less than 20%. The upper troposphere/lower stratosphere shows mean high biases of near 20%, extending from 100mb-300mb, below 300mb, the RAQMS shows low biases of less than 10%. The RAQMS analysis captures the majority of the observed variance enhancement in the lower stratosphere and continental boundary layer but also shows large RMS errors (near 50% at 200mb). These RMS errors are due to vertical displacement of filaments of high and low ozone associated with stratosphere-troposphere exchange processes.

Figure 8 shows comparisons between RAQMS surface ozone and ozone measurements from the EPA AIRNOW network [Wayland, 2002]. These maps show mean statistics based on timeseries analysis for the individual AIRNOW stations. The median temporal correlation between the 6 hourly RAQMS prediction and coincident 1hour AIRNOW measurements is .72 (not shown), and largely reflects the diurnal cycle in surface ozone. To assess the ability of the RAQMS ozone analysis to capture daily variations in surface ozone we consider correlations between the diurnally averaged RAQMS analysis and coincident AIRNOW measurements. The median correlation between diurnally averaged RAQMS and AIRNOW data is .59 with lowest correlations in the diurnally averaged ozone found over West Virginia, Southern California, and the western mountain states. These low correlations are most likely associated with unresolved local variations in dry deposition due to local variations in topography and emissions.

To assess the ability of the RAQMS ozone analysis to capture daytime photochemistry we compiled station-by-station mean biases at 18Z, which is mid-day over much of the central and eastern US. 18Z mean biases are generally positive with a

median value of 15.5 ppbv. 18Z mean biases are largest within the Mississippi and Ohio River valleys. The daytime mean biases may associated with overestimates in surface ozone production, overestimates in boundary layer O3 entrainment, assimilation of TOMS column ozone (which occurs during the 18Z assimilation cycle over North America), or overestimates in the initial (morning) surface ozone. Overestimates in surface ozone production would suggest excess NOx, however column NO2 is actually underestimated (particularly in urban areas) based on the RAQMS/SCIAMACHY comparison. Entrainment is also unlikely to account for the 18Z bias since boundary layer O3 is actually underestimated (in the mean) based on the RAQMS/IONS comparison. This leaves overestimates in the initial (morning) surface ozone or TOMS column ozone assimilation as the most likely reasons for the mean daytime bias. Nighttime (00Z) biases show a similar pattern with median values of 18.1 ppbv. The 00Z biases are frequently associated with underestimates in nighttime titration of ozone, which is a near-surface phenomena that is not accurately captured within RAQMS.

3.3 Comparison with DC8 insitu measurements

Figure 9 shows comparisons with insitu CO, O3, NO2, PANS, and HNO3 data obtained by instruments onboard the NASA DC8 during all flights during INTEX-A as well as observationally constrained photochemical steady state calculations from the LaRC boxmodel [Crawford et al., this issue]. These comparisons were made by interpolating the RAQMS chemical fields onto the DC8 flight track and sampling the model at the frequency of the insitu measurements, then binning the modeled and measured values into 50mb pressure bins. The median (vertical profile), 50^{th} (bar) and

90^{th} (whisker) percentiles of the modeled and observed distributions within each pressure bin are shown. The modeled CO is 5-10 ppbv lower than observed except at 950mb where the model is approximately 20 ppbv higher than insitu measurements. Predicted and observed column amounts, obtained by integrating the median number densities between 1000 and 250 mb, are $1.8x10^{18}$ and $1.82x10^{18}$ mol/cm^2, respectively. The 1-2% agreement between the predicted and insitu median column amounts is consistent with the comparison between the RAQMS and MOPITT CO columns, which showed median biases of 1.2% over the continental US. The modeled O3 is within 10ppbv below 400mb and approximately 20ppbv higher than the observations above 400mb. The column densities obtained from integration of the median analyzed and insitu ozone profiles are 46.6 and 42.2 DU, respectively, resulting in a 10% error in the median ozone column estimated from the aircraft measurements. The 20-25% differences between the RAQMS ozone analysis and insitu mixing ratios in the upper troposphere are consistent with the comparison between RAQMS and the IONS ozonesonde data, suggesting that the analyzed tropospheric O3 column is within 10% of the actual column over the continental US. The modeled NO2 is approximately 50ppbv low (factor of 2) relative to the measurements at 300mb and larger than observed below 800mb. The predicted median NO2 mixing ratio is a factor of 2 larger than observed at 950mb. Column NO2 densities, based on integration of the predicted and observed median profiles, are $1.74x10^{15}$ and $1.34x10^{15}$ mol/cm^2, respectively, resulting in a 30% bias in the median NO2 column estimated from the aircraft measurements. The high bias in median NO2 column density, relative to the insitu data, is not consistent with the 46% negative median bias found relative to SCIAMACHY tropospheric NO2 column densities. The differences between

the results of the SCIAMACHY and insitu verification studies could only arise from low biases in the RAQMS NO2 mixing ratios below the 1000ft minimum altitude of the DC8. Such biases are very likely within urban boundary layers (which were not sampled by the DC8) and could also result from underestimates in large soil NOx emissions associated with fertilizer application and subsequent precipitation [Bertram, et al., 2005, Juegle, et al., 2005] in the western US. Total PANs (peroxynitrates) are within 50pptv of the observed mixing ratios except for near 800mb where the modeled Total PAN (PAN+HNO4) is low by 75pptv. HNO3 is low by 200 – 400 pptv below 600mb and high by 150 pptv at 300mb. The modeled ozone P-L is in very good agreement with observationally constrained photochemical steady state calculations except at 300mb where the modeled P-L (1 ppbv/day) is low by a factor of 2. This underestimate in ozone P-L is consistent with factor of 2 underestimate of NO2 at this altitude. The fact that the model ozone overestimates are associated with overestimates in HNO3 and underestimates in P-L, NO2 and TOTPANS, suggests that the model overestimates stratospheric influences (high O3, HNO3), underestimates convective influences (P-L, NO2, PAN), or both in the upper troposphere.

4. Global and Continental US estimates of Ozone and NOy STE

The preceding discussion highlights the important role that stratospheric-tropospheric exchange (STE) plays in determining the distribution of ozone and NOy (primarily HNO3) in the upper troposphere during INTEX-A. In this section, we follow the discrete approach outlined by Pierce et al, [2003] to estimate the contribution of STE to the global distribution of upper tropospheric ozone during INTEX-A. In Pierce et al.,

[2003] the regional component of RAQMS was used to determine discrete, cross-tropopause ozone fluxes over S.E. Asia during the NASA TRACE-P mission. The discrete cross tropopause flux was estimated by computing instantaneous horizontal and vertical fluxes out of tropospheric grid-boxes that were adjacent to the model tropopause, using the WMO thermal tropopause definition. Here we apply the same approach using the global component (UW-Hybrid dynamical core) of RAQMS. The UW-Hybrid model is formulated in hybrid isentropic-eta coordinates and consequently grid boxes are defined in the vertical by potential temperature surfaces above 345K, or roughly the mid-latitude tropopause. This hybrid isentropic-eta formulation of the UW-Hybrid dynamical core allows us to explicitly compute the isentropic (quasi-horizontal) exchange of stratospheric and tropospheric air across the tropopause break, which extends from roughly 345K to 380K in potential temperature. This region of the lower stratosphere, bounded by the tropopause and the 380K potential temperature surface, is coupled to the upper tropical troposphere through isentropic exchange of mass, momentum, and trace gases.

Figure 10 shows the zonally averaged cross tropopause ozone and NOy fluxes during the period from July 01- August 15, 2004. The ozone and NOy fluxes across the 380K potential temperature are also shown. NOy fluxes are determined by computing the instantaneous 6 hourly fluxes of individual components of NOy (NO+NO2+NO3+HNO3+HNO4+2*N2O5+ClNO3+PAN+organic nitrates) and then adding them together. The RAQMS first guess odd oxygen (Ox) is used to compute the 6hourly ozone fluxes to assure dynamical consistency between the Ox and forecasted winds. The time averaged cross tropopause ozone and NOy fluxes is determined by

averaging 6 hourly calculations of horizontal (isentropic) and vertical (diabatic) fluxes, and movement (in altitude) of the tropopause. Since the 380K surface is a model level, the horizontal velocities at 380K are parallel to the 380K surface and the time averaged ozone and NOy flux at 380K only includes vertical fluxes plus movement (in altitude) of the 380K surface.

In the tropics, the ozone and NOy fluxes are upward (positive) with net transport through the tropopause and 380K potential temperature surface into the lower stratosphere. This transport is driven by radiative heating and upward diabatic vertical motion. In polar regions, the diabatic transport of ozone and NOy across the 380K potential temperature surface is downward and driven by radiative cooling. The net transport of ozone and NOy across the polar tropopause is also downward, but it occurs through the combined effects of downward diabatic motion and secular changes (increases) in the altitude of the polar tropopause, which compensate for net horizontal (isentropic) fluxes of ozone and NOy into the middle world. At the tropopause break, horizontal (isentropic) ozone and NOy fluxes from the troposphere into the stratosphere dominate.

These results are consistent with mass flux estimates by Schoeberl [2004] who used explicit calculations of the diabatic fluxes through the 380K potential temperature surface and tropopause, along with mass tendencies within the middle world, to estimate adiabatic (isentropic) exchange through the tropopause. He found net adiabatic fluxes across the tropopause were positive (into the middle world) throughout the year. However, because the adiabatic term was obtained as a residual, he was not able to determine the latitudinal distribution of the adiabatic cross tropopause flux. The RAQMS

analysis shows that the adiabatic flux is largest at the tropopause break. This net flux (from above and below) of trace gases into the middle world on the poleward side of the tropopause break introduces the possibility for accumulation of ozone and NOy with both stratospheric and tropospheric origins within this region.

Figure 11 shows the zonally averaged cross tropopause ozone and NOy fluxes during the period from July 01- August 15, 2004 for the Continental US budget domain. The regional ozone and NOy fluxes across the 380K potential temperature surface are also shown. The cross tropopause fluxes of ozone and NOy over the Continental US are dominated by quasi-horizontal (isentropic) transport into the middle world. The both ozone and NOy show peak troposphere to stratosphere ozone fluxes at 45oN with the cross tropopause NOy flux being dominated by transport of HNO3. The fluxes of ozone and NOy across the 380K potential temperature surface are largest on the northern boundary of the budget domain and are dominated by downward (diabatic) transport into the middle world. These results are consistent with the global flux estimates for this latitude band and suggest that there should be an accumulation of ozone and NOy, some of tropospheric and some of stratospheric origin, in the lower stratosphere over the Continental US during INTEX-A. The net upward flux of ozone and NOy at the tropopause within the Continental US budget domain suggests that the stratospherically influenced tropospheric air observed in the IONS composite must have entered the troposphere poleward of the Continental US domain, where net cross tropopause fluxes are downward.

5. Ozone and NOy budgets over the Continental US

5.1 Ozone Budget analysis

Ozone assimilation reduces errors in the budget analysis by providing an improved estimate of ozone within the Continental US budget volume. However, assimilation introduces non-physical changes in ozone that must be isolated from the physical and chemical processes accounted for in the RAQMS simulation. To isolate the influences of assimilation in the budget calculations we use the RAQMS first guess ozone distributions to compute the lateral and diabatic fluxes. Since the first guess ozone has been advected for the previous 6 hours with forecasted wind fields and experienced the effects of the predicted photochemistry, the first guess is dynamically and chemically consistent. The ozone analysis increment is treated as a separate (although non-physical) budget term. This approach allows us to isolate the effects of assimilation in the budget calculations.

Figure 12 shows the time averaged zonal mean distribution of Continental US ozone, net P-L, convective mixing tendencies, and the mean absolute value of the assimilation increment. The mean location of the middle world, bounded by the thermal tropopause and 380K potential temperature surface, is also indicated. Mean ozone mixing ratios are above 80ppbv in the northern upper troposphere and range from 200-350 in the middle world. Lower tropospheric ozone mixing ratios are less than 55 ppbv, with no clear indication of a surface enhancement. Time averaged upper tropospheric net ozone production (P-L) reaches 4.0 ppbv/day at 10 km and 30N, and shows net photochemical destruction below 7 km in the southern portion of the domain. Net photochemical production reaches 10ppbv/day in the Continental US boundary layer. Deep convection in the southern part of the domain leads to upper level detrainment of low ozone mixing

ratios within convective updrafts, resulting in upper tropospheric ozone reductions of nearly 7ppbv/day. This convective ozone sink is localized near the region of largest net photochemical production, suggesting lighting NOx emissions and convective transport of boundary layer NOx emissions play an important role in the upper tropospheric ozone production. Lateral detrainment of higher ozone mixing ratios during deep convection leads to mid-tropospheric increases in ozone at a rate of 5 ppbv/day. Shallow convection near 40N results in entrainment of higher ozone mixing ratios associated with ozone production within the continental boundary layer. This low level entrainment and subsequent convective lofting leads to localized convectively induced ozone sinks of up to 2.0 ppbv/day in this region. The RMS effects of the ozone assimilation are less than 1% over much of the troposphere, with localized regions below 2km in the northern part of the budget domain showing upwards of 2% RMS changes. Relatively uniform assimilation increments of 2% or more are found just above the tropopause and are a result of the assimilation of the solar occultation and limb scattering measurements.

Figure 13 shows the time averaged ozone number densities for each of the lateral boundaries of the Continental US domain. The time averaged tropopause and 380K potential altitudes are also shown. On the western boundary the ozone number densities are very low below 2km, reflecting the influence of clean maritime air. Mid-tropospheric ozone enhancements are found along each domain boundaries. Within the middle world, there are local maxima in ozone number densities near the northern edges of both the western and eastern boundaries, as well as over the western half of the northern boundary. These local maxima are evidence for the accumulation of ozone within the middle world and are a result of the global scale vertical and horizontal flux convergence

poleward of the tropopause break discussed in Section 4. The largest local enhancements in ozone number densities are found in the middle world along the western portion of the northern boundary. These ozone enhancements are associated with an upper tropospheric trough pattern which persisted during much of INTEX-A. The signature of this upper tropospheric trough is evident in the lower time averaged tropopause altitudes along the western portion of the northern boundary.

Figure 14 shows the time averaged ozone fluxes, in mol/cm^2/sec, for each of the lateral boundaries of the Continental US domain. Negative values denote fluxes into the Continental US while positive values denote export out of the Continental US. The largest ozone fluxes (both into and out of the Continental US) occur along the eastern and western boundaries and arise due to the prevailing westerly winds along the northern portion of the Continental US. These ozone fluxes maximize in the middle world, and are coincident with local maxima in ozone number densities shown in Figure 13. There is a reversal of the fluxes on the eastern and western boundaries over the southern US associated with the prevailing stratospheric easterlies near 20km. The ozone export along the eastern boundary is significantly larger than ozone import along the western boundary, leading to net ozone export out of the Continental US. The alternating pattern of middle world ozone fluxes along on the northern boundary is a consequence of meridional transport within the upper level trough, with net import on the western flank and export on the eastern flank. The ozone fluxes along the southern boundary are very small.

The large time averaged lateral fluxes, coupled with flux convergence associated with upward STE and downward diabatic transport into the middle world, suggest that

neglecting this region in the US ozone budget could lead to significant underestimates in the actual export during INTEX-A. Consequently, in the subsequent budget analysis, we consider the 380K potential temperature surface to be the top of the budget domain. Figure 15 shows the time series of the accumulated changes in Continental US ozone associated with ozone production, 380K diabatic fluxes, lateral fluxes, ozone assimilation, and dry deposition. The actual and computed accumulation, determined from the sum of the individual budget terms, is also shown. The initial Continental US ozone burden below 380K was 15.6 Tg. Variations in the total ozone below 380K are on the order of 2 Tg with small (<1 Tg) net changes in Continental US ozone during INTEX-A. The close agreement between the actual and computed accumulation during INTEX-A indicates low accumulative errors in the budget calculation.

Net photochemical production is the dominant source of changes in Continental US ozone during INTEX-A, with accumulated insitu ozone production of 7.63 Tg. However, photochemical production slows down significantly after Julian Day 198 (July 15), as reflected in the much slower accumulation due to ozone photochemistry during the later half of July, and becomes negative in August, as reflected in the decline in ozone accumulation due to Net P-L after Julian day 220. The reductions in photochemical ozone production are attributed to the anomalously cold weather pattern during these periods. August 2004 was the 7th coldest on record with cold outbreaks occurring during July 26-30 and August 10-16 [Fuelberg et al, this issue]. These cold air outbreaks are associated with increased surface winds which lead to efficient boundary layer ventilation and reduced accumulation of ozone precursors. US EPA air quality statistics for 92 major metropolitan areas in the continental US show that 2004 had the fewest days with ozone

Air Quality Indexes over 100 (corresponding to 8 hour average ozone mixing ratios greater than 85 ppbv) during the last 15 years (1990-2004). The reduction was highly significant. When all US metropolitan areas are considered the number of ozone AQI>100 days in 2004 was 66% less than the 15 year median value. If we exclude California, Dallas, and Houston the number of ozone AQI>100 days in 2004 was 82% less than the 15 year median.

The rate of ozone loss due to dry deposition remains nearly constant throughout the INTEX-A period and is the dominate sink of ozone within the budget volume. Accumulated losses due to dry deposition (7.39 Tg) nearly balance net photochemical production over the Continental US during INTEX-A. Lateral ozone fluxes result in accumulative reductions (net export) of 3 Tg during INTEX-A, however, most of this export occurs prior to Julian Day 201 (July 18th). After July 18th there were a series of anomalously deep upper level troughs over the US [Fuelberg, et al, this issue] which contributed to the significant week to week variability in the lateral fluxes during the latter half of July and first half of August. Diabatic fluxes across the 380K surface result in the import of 3 Tg of stratospheric ozone to the Continental US domain during the INTEX-A time period.

There is a significant reduction in the rate of accumulation of stratospheric ozone within the Continental US domain after Julian day 197 (July 15th) corresponding to the beginning of the assimilation of SAGE III limb scattering measurements. As was shown in Section 3.2, assimilation of SAGE limb scattering measurements had a positive impact on the RAQMS vs IONS ozonesonde statistics by reducing high biases in the region of the upper troposphere with significant stratospheric influences. Assimilation increments

during the SAGE limb scattering period (July 15th-July 31st) result in a net loss of 3 Tg of ozone over the continental US, which is comparable in magnitude to the total ozone export during INTEX-A. After July 31st the assimilation of the SAGE limb scattering measurements stops and assimilation of TOMS column ozone only results in systematic increases in ozone within the budget volume until the SAGE limb scattering assimilation is resumed on August 12th. The assimilation of SAGE III limb scattering measurements also impacts the estimates of lateral fluxes, which maximize in the middle world. This is reflected in the anti-correlation between the accumulated effects of assimilation and lateral fluxes after July 15th. Whether changes in the lateral fluxes are associated with the inclusion of SAGE III limb scattering data in the assimilation or changes in the upper tropospheric circulation during the latter part of INTEX-A is a difficult question to answer. Future budget studies could address this question by conducting budget analysis with and without assimilation.

The majority of the export from the Continental US domain occurs in the middle world, consequently, the net import of approximately 3 Tg of stratospheric ozone across the 380K potential temperature surface is likely to account for the majority of the 3 Tg of ozone that is exported during INTEX-A. To obtain an estimate of the export of ozone that was photochemically produced within the Continental US domain during INTEX-A we need to remove the stratospheric contribution from the accumulated lateral export. This results in 9.4e9 g of ozone photochemically produced over the US and exported during INTEX-A, which is a negligible fraction of the total export.

5.2 NOy Budget analysis

The export of total reactive nitrogen (NOy) from the continental US is equally as important as the export of ozone, since availability of nitrogen oxides ($NO+NO_2$) determine subsequent ozone production [Chameides et al., 1992]. In this section we discuss results from Eulerian budget calculations focusing on NOy. Figure 16 shows the time averaged zonal mean distribution of Continental US NOy, lighting NOx production, convective exchange of NOy, and NOy wet deposition. The zonal mean surface NOy is over 4 ppbv and is dominated by localized NOx enhancements due to emissions and HNO3. There is a pronounced tongue of elevated NOy extending down from the mid-latitude tropopause that has significant stratospheric influences. Since the cross tropopause NOy flux is from the troposphere to the stratosphere within the Continental US budget domain, these NOy enhancements must arise due to STE outside of the Continental US. Al-Saadi et al. [this issue] show much of the stratospherically influenced air within the continental US had it's origins over the central Pacific and S. E. Asia. Cloud top detrainment of lightning NOx emissions in the southern portion of the domain results in NOy production of 0.25 ppbv/day in the upper troposphere (7-10km), with nearly equal amounts below 2km associated with outflow from convective downdrafts [Pickering, 1998]. Convective mixing entrains continental boundary layer NOy at a rate of 2 ppbv/day where it is either immediately rained out (for highly soluble species such as HNO3) or convectively lofted (for less soluble species such as PAN) and deposited between 5 and 10 km. In contrast to ozone, convective exchange increases free tropospheric NOy mixing ratios at a rate of 0.15 ppbv/day. This is a consequence of the different vertical gradients in NOy and ozone below 10 km.

Figure 17 shows the time averaged NOy number densities for each of the lateral boundaries of the Continental US domain. The distribution of middle world NOy and ozone number densities (Figure 13) are very similar with local maxima on the northern edges of the western and eastern boundaries and on the eastern edge of the northern boundary. These local maxima are primarily HNO3, and result from net flux converge within this region. However, in the troposphere there are significant differences between the ozone and NOy number densities on the lateral boundaries. The largest NOy number densities are found below 5km on the northern boundary and below 2 km on the eastern boundary. The enhancements in NOy on the northern boundary are primarily HNO3 and PAN and are due to transport from the Alaskan wild fires [Al-Saadi et al, this issue]. The large local enhancements in NOy number densities below 2km along the eastern boundary are primarily due to HNO3 as are the low level enhancements in NOy on the western boundary. Mid tropospheric enhancements in NOy number densities along the eastern and southern boundaries are primarily due to PAN. Figure 18 shows the time averaged NOy fluxes, in mol/cm^2/sec, for each of the lateral boundaries of the Continental US domain. As with the number densities, the distribution of NOy fluxes in the middle world are similar to the ozone fluxes (Figure 14) and are dominated by fluxes of HNO3. In the troposphere, there is significant NOy import (negative fluxes) on the northern boundary near 5km. These fluxes are primarily due to transport of HNO3 and PAN from the Alaskan wildfires. The NOy export (positive fluxes) on the northern part of the eastern boundary extends well into the troposphere. This is due to export of PAN, which maximizes near 7km along the northern portion of the eastern boundary. The localized export of NOy below 2 km at 45N is primarily composed of HNO3.

While there is significant complexity in the way that NOy species are partitioned among the various regions of import and export the evolution of the accumulated changes in Continental NOy is actually quite simple due to the fact that it's primary source is surface emissions, which are held constant throughout the simulation. Figure 19 shows the time series of the accumulated changes in Continental US NOy (expressed in Tg of nitrogen) due to sources (industrial plus aircraft and soil emissions, lightning emissions), sinks (wet and dry deposition) and transport (380K diabiatic fluxes and lateral fluxes). The actual and computed accumulation, determined from the sum of the individual budget terms, is also shown. The initial Continental US NOy burden below 380K was 0.05 Tg. The actual and computed NOy accumulation over the Continential US were very small during INTEX-A, as are the 380K diabatic fluxes. The Continental US NOy budget shows accumulated NOy emissions of 0.94 Tg nitrogen (with less than 20% due to lightning NOx production) and accumulated depositional loss of 0.69 Tg nitrogen (.47 Tg wet, .22 dry), resulting in a net export of 0.23 Tg of nitrogen and an export efficiency of 24%.

6. Discussion

Liang et al. [1998] (here after referred to as L98) used sensitivity experiments based on differences between two continental-scale photochemical model simulations (one with and one without US NOx emissions) to estimate seasonally averaged fluxes of ozone and NOy. The summer season (JJA) ozone export from the Continental US boundary layer in the standard (with US NOx) simulation was 1.8 Gmol/day, while difference between the standard simulation and one without US NOx emissions, referred

to as “pollution ozone” was 6.5 Gmol/day. Li et al. [2004] (here after referred to as L04) used the GEOS-CHEM model sensitivity experiments to estimate US ozone export out of the Continental US boundary layer during September 1997 and found “pollution ozone” export of 5 Gmol/day, consistent with the Fall (SON) estimates by L1998. Furthermore, L04 showed that nearly 70% of the ozone production associated with Continental US NOy export out of the boundary layer occurs directly over North America, referred to as “near field ozone production”, and would therefore be included in the RAQMS INTEX-A Continental US budget calculations presented here.

The L98 horizontal Continental US domain size was similar to the current INTEX-A budget domain. Applying the JJA L98 standard simulation export rate over the 46 day INTEX-A budget period would result in 3.97 Tg of ozone exported through the continental US boundary layer, comparable to our estimates of net export, however, as discussed earlier, the RAQMS INTEX-A ozone export is of stratospheric origin. Applying the JJA L98 “pollution ozone” export rate over the 46 day INTEX-A budget period would result in 14.35 Tg of US ozone exported through the continental boundary layer, which is significantly larger than our estimates of net export of photochemically produced ozone from the Continental US budget domain during INTEX-A.

Direct comparisons of the INTEX-A Continental US photochemical ozone export and the L98 and L04 “pollution ozone” estimates are not appropriate since the “pollution ozone” reflects the fact that without emissions, the Continental US would be a strong sink of ozone due to photochemical losses and dry deposition near the surface. However, because of the large discrepancies between the L98 standard simulation and the RAQMS estimates of ozone export during INTEX-A, some discussion is warranted.

The main reason for the large differences between the current estimate of US photochemical ozone export during INTEX-A and the L98 standard simulations results is the anomalously cold surface temperatures during August 2004, which actually resulted in net photochemical ozone loss within the Continental US domain during the first 2 weeks of August. If we restrict our budget calculations to July 01-15, we obtain a net export of photochemically produced ozone of 1.4 Tg. This export is in good agreement with the ozone export that would be obtained by applying the L98 JJA seasonal rate of 1.8 Gmol/day from the standard simulation over this same period (1.3Tg). However, the RAQMS ozone budget includes ozone production above the continental boundary layer while the L98 does not. The accumulated ozone P-L within the budget domain from July 1-15 is 3.84 Tg. This is 85% of the accumulated continental boundary layer P-L that would be obtained for the same 15 day period using seasonally averaged P-L rates from the L98 standard simulation. The RAQMS simulation removes 2.23 Tg, or 58% of the ozone produced over the Continental US due to dry deposition during the period from July 1-15. In contrast, dry deposition removes only 33% of the ozone produced over the Continental US in the L98 standard simulation.

As shown in section 3.3, the RAQMS estimates in P-L are in good agreement with observationally constrained photochemical box model estimates during INTEX-A, indicating that the current estimates of P-L are reasonable. Talbot et al., [2005] provide estimates of nocturnal ozone dry deposition during the summer based on 3 years (2001-2003) of ozone measurements at the Harvard Forest site. They find median nocturnal deposition rates of 11 ppbv/night, which are considered representative of heavily forested regions in New England. This estimate compares very well with median RAQMS

nighttime (00Z-12Z) averaged ozone deposition velocities over New England (11.29 ppbv/night) during INTEX-A.

Taken as a whole, these comparisons indicate that the photochemical ozone export from the Continental US budget domain during July 1-15, 2004 was consistent with the L98 standard simulation results assuming that the near field ozone production due to NOy export through the continental US boundary layer was small. However, due to anomalously cold surface temperatures and resulting net ozone destruction during the first two weeks of August, the export of photochemically produced ozone was insignificant compared to the export of stratospheric ozone in the upper troposphere/lower stratosphere over the Continental US during the overall INTEX-A time frame (July 01-August 15, 2004).

The agreement between the RAQMS INTEX-A and J98 based estimates of Continental US NOy export over the INTEX-A time frame is quite good. Recall that the INTEX-A Continental US NOy budget shows accumulated NOy emissions of 0.94 Tg nitrogen and accumulated depositional loss of 0.69 Tg nitrogen (.47 Tg wet, .22 dry), resulting in a net export of 0.23 Tg of nitrogen and an export efficiency of 24%. Applying the rates from L1998 NOy budget estimates to the INTEX-A time period results in 0.86 Tg of nitrogen emissions, accumulated depositional loss of 0.64 Tg nitrogen (.24 Tg wet, 0.4 dry), net export of 0.23 Tg of nitrogen and an export efficiency of 27%, all of which are within 10% or less of the INTEX-A estimates. Wet deposition accounts for the majority of the NOy depositional loss based on the RAQMS budget calculations where as dry deposition accounts for the majority of the L1998 depositional loss. This is to be expected since the RAQMS budget domain includes the entire troposphere and

consequently the full vertical extent of wet deposition within convective cells is included in the NOy budget. The RAQMS budget analysis indicates that NOx+PAN accounts for 54% of the NOy exported out of the Continential US during INTEX-A, which is 15% lower than the L1998 estimate of 63%. This difference is due to the additional contributions from HNO3 export in the middle world which is included in the RAQMS NOy budget calculations. Both INTEX-A and J1998 export efficiencies are slightly higher than the L2004 Eulerian estimates of 20% during September 1997.

7. Summary and Conclusions

We have used aircraft, satellite, surface, and ozonesonde measurements to verify a 6 week RAQMS simulation of the unified troposphere-stratosphere chemistry during the INTEX-A time period. These verification studies show that RAQMS captures the main features of the global tropospheric distribution of ozone, carbon monoxide, and NOy with reasonable fidelity, although RAQMS underestimates the median tropospheric NO2 distribution relative to SCIAMACHY measurements and overestimates the impact of the Alaskan wild fires on column CO relative to MOPITT. Comparisons with insitu airborne measurements shows that RAQMS reproduces the statistical characteristics of the insitu observations (median and variances) with reasonable accuracy (generally within 20%) although RAQMS tends to overestimate stratospheric influences and underestimate convective influences in the upper troposphere over the continental US (high biases in ozone and HNO3 and low biases in ozone P-L and NO2 above 400mb). Based on comparisons with ozonesondes from the IONS network, the assimilation of satellite based profile and column ozone measurements has been shown to have a positive impact on the

RAQMS upper tropospheric/lower stratosphere ozone analyses (mean biases of 20%), particularly during the period when higher density SAGE III limb scattering measurements were available over the Continental US. Comparisons with surface ozone measurements from the US EPA AIRNOW network show that the RAQMS surface ozone analysis captures the daily variability in surface ozone over most of the eastern US very well, with correlations between 24hr averaged measurements and the RAQMS analysis generally near 0.8. However, due to local variations in topography and emissions, the daily correlations over the Central Appalachians are considerably lower (0.2-0.4). The RAQMS surface ozone analysis shows a systematic high bias (18ppbv at night, 15ppbv during the day) relative to AIRNow surface measurements, which is attributed to underestimates in nocturnal titration due to underestimates of surface NOx in urban environments.

Eulerian ozone and NOy budgets during INTEX-A show that the majority of the Continental US export occurs in the upper troposphere/lower stratosphere poleward of the tropopause break. The localized ozone and NOy export was shown to occur due to convergence of tropospheric and stratospheric air in this region. These results suggest that providing a robust assessment of the influence of the Continental US on the global environment requires accurate representation of the long-range transport and mixing processes within this region. Continental US photochemically produced ozone was found to be a minor component of the total ozone export, which was dominated by stratospheric ozone that was diabatically transported into the middle world during INTEX-A. The unusually low photochemical ozone export is attributed to anomalously cold surface temperatures during the latter half of the INTEX-A mission. Efficient boundary layer

venting associated with cold air outbreaks during late July and mid August tended to reduce accumulation of ozone precusors resulting in net ozone loss during the first 2 weeks of August. Eulerian NOy budgets during INTEX-A where shown to be very consistent with previously published estimates. The NOy export efficiency was estimated to be 24%, with NOx+PAN accounting for 54% of the total NOy export during INTEX-A.

References:

Al-Saadi, J. A., R. B. Pierce, T. D. Fairlie, T. K. Schaack, C. Kittaka, D. R. Johnson, T. H. Zapotocny, M. Avery, A Lagrangian Characterization of the Sources and Chemical Transformation of Air Influencing the US and Europe during the 2004 ICARTT/INTEX-A Campaign, this issue

Atherton, C. S. et al., Three-dimensional global modeling studies of the transport and photochemistry over the North Atlantic Ocean, J. Geophys. Res., 101, 29,289-29,304, 1996.

Avery, M. A. et al., Impact of multi-scale dynamical processes and mixing on the chemical composition of the upper troposphere and lower stratosphere during INTEX-A, this issue.

Bertram, T. H., A. Heckel, A. Richter, J. P. Burrows, and R. C. Cohen, Satellite measurements of daily variations in soil NOx emissions, Geophys. Res. Lett. Doi:10.1029/2005GL024640, 2005

Bian, H. and M. J. Prather, Fast-J2 Accurate simulation of stratospheric photolysis in global chemical models, J. Atmos. Chem.,41, 281-296, 2002.

Buker, M. L., M. Hitchman, G. Tripoli, R. B. Pierce, E. V. Browell, M. A. Avery, and J. Al-Saadi, Convective initiation of long-range ozone transport during INTEX, this issue.

Carslaw, K. S., B. Luo, T. Peter, An analytic expression for the composition of aqueous HNO3 - H2SO4 stratospheric aerosols including gas phase removal of HNO3, Geophys. Res. Lett., 22(14), 1877-1880, 10.1029/95GL01668, 1995.

Carter, W., Isoprene chemistry for the RADM-2 mechansim, adaptation of the 4-product mechanism, 1997, http://pah.cert.ucr.edu/~carter/bycarter.htm#endarts.

Chameides, W. L., et al. (1992), Ozone precursor relationships in the ambient atmosphere, *J. Geophys. Res.*, *97*, 6037–6055.

Chipperfield, M. P., Multiannual simulations with a three-dimensional chemical transport model, J. Geophys. Res., 104(D1), 1781-1806, 10.1029/98JD02597, 1999.

Cofer III, W.R., E.L. Winstead, B.J. Stocks, D.R. Cahoon, J.G. Goldammer, and J.S. Levine (1996a) Composition of Smoke from North American Boreal Forest Fires, in Fire in Ecosystems of Boreal Eurasia, J.G. Goldammer, and V.V. Furyaev, pp. 465-475, Kluwer Academic Publishers, Dordrecht.

Cofer, W.R., III, E.L. Winstead, B.J. Stocks, L.W. Overbay, J.G. Goldammer, D.R. Cahoon, Jr., and J.S. Levine (1996b) Emissions from Boreal Forest Fires: Are the Atmospheric Impacts Underestimated?, in Biomass burning and global change, J.S. Levine, pp. 834-839,MIT Press, Cambridge, Mass.

Crawford, J., et al., Summertime ozone production over North America during INTEX-A based on observed and modeled photochemistry, this issue.

Crawford, J., D. Davis, J. Olson, G. Chen, S. Liu, G. Gregory, J. Barrick, G. Sachse, S. Sandholm, B. Heikes, H. Singh, and D. Blake, Assessment of upper tropospheric HOx sources over the tropical Pacific based on NASA GTE/PEM data: Net effect on HOx and other photochemical parameters, J. Geophys. Res., 104, 16255-16273, 1999.

Dentener F.J. and P.J. Crutzen, Reaction of N2O5 on tropospheric aerosols: impact on the global distributions of NOx, O3 and OH, J. Geophys.Res., 98, 7149-7163, 1993

Duncan B. N., I. Bey (2004), A modeling study of the export pathways of pollution from Europe: Seasonal and interannual variations (1987–1997), J. Geophys. Res., 109, D08301, doi:10.1029/2003JD004079.

Errico, R. M., Meeting Summary, Workshop on Assimilation of Satellite Data, Bull. Amer. Met. Soc., 80, 463-471, 1999.

Fishman, J. and A. E. Balok, Calculation of daily tropospheric ozone residuals using TOMS and empirically improved SBUV measurements: Application to an ozone pollution episode over the eastern United States, J. Geophys. Res., 104, 30,319-30,340, 1999.

Fuelberg, H. E. M. Porter, C. M. Kiley, D. Morse, A meteorological overview of the INTEX-A period, this issue.

Galbally , I.E. and C.R. Roy, Destruction of ozone at the earths' surface, Q.J.R. Meteorol. Soc., 106, 599-620, 1980.

Gery, M.W., G.Z. Whitten, J.P. Killus, and M.C. Dodge, A photochemical kinetics mechanism for urban and regional scale computer modeling, J. Geophys. Res., 94, 12925-12956, 1989.

Horowitz, L. W., J. Liang, G. M. Gardner, and D. J. Jacob (1998), Export of reactive nitrogen from North America during summertime: Sensitivity to hydrocarbon chemistry, *J. Geophys. Res.*, *103*, 13,451–13,476

J. R. Holton, P. H. Haynes, M. E. McIntyre, A. R. Douglass, R. B. Rood, L. Pfister, Stratosphere-Troposphere Exchange, Rev. Geophys. 33 (4), doi:10.1029/95RG02097, 1995

Jacob, D. J., et al., Factors Regulating Ozone Over the United States and Its Export to the Global Atmosphere, J. Geophys. Res., 98, 14,817-14,826, 1993.

Jaegle L, L., L. Steinberger, R.V. Martin, and K. Chance, Global partitioning of NOx sources using satellite observations: Relative roles of fossil fuel combustion, biomass burning and soil emissions, Faraday Discussions, 130, 407-423, doi:10.1039/b502128f, 2005.

Jeuken, A.B.M., H.J. Eskes, P.F.J. van Velthoven, H.M. Kelder and E.V. Hólm, 1999: Assimilation of total ozone satellite measurements in a three-dimensional tracer transport model. J. Geophys. Res., 104, 5551-5563.

Jing, P., D. M. Cunnold, H. J. Wang, and E.-S. Yang, Isentropic Cross-Tropopause Ozone Transport in the Northern Hemisphere, J. Atmos. Sci., 61, 1068-1078, 2004.

Kasibhatla, P. S., H. Levy II, and W. J. Moxim (1993), Global NO_x, HNO_3, PAN, and NO_y distributions from fossil fuel combustion emissions: A model study, *J. Geophys. Res.*, *98*, 7165–7180.

Kirchner, F. and W. R. Stockwell, *Effect of peroxy radical reactions on the predicted concentrations of ozone, nitrogenous compounds, and radicals*, J. Geophys. Res., 101(D15), 21007, 1996.

Knapp, K. G., et al., Observation of the transport of polluted air masses fro the northeastern United States to Cape Sable Island, Nova Scotia, Canada, during the 1993 NARE summer intensive, J. Geophys. Res. 103, 13,399-13,411, 1998.

Lamarque, J. F., et al., Assimilation of Measurement of Air Pollution from Space (MAPS) CO in a global three-dimensional model, J. Geophys. Res., 104, 26,209-26,218, 1999.

Levy, H. II, J.D. Mahlman, W.J. Moxim, and S.C. Liu, Tropospheric Ozone: The role of transport, J. Geophys. Res., 90, 3735-3772, 1985.

Liang, J. et al., Seasonal budgets of reactive nitrogen species and ozone over the United States, and export fluxes to the global atmosphere, J. Geophys. Res., 103, 13,435-13,450, 1998.

Liu, H., D. J. Jacob, I. Bey, R. M. Yantosca, Constraints from ^{210}Pb and ^{7}Be on wet deposition and transport in a global three-dimensional chemical tracer model driven by assimilated meteorological fields, J. Geophys. Res., 106(D11), 12109-12128, 2001.

Lurmann, F.W., A.C. Lloyd, and R. Atkinson, A chemical mechanism for use in long-range transport/acid deposition computer modeling, J. Geophys. Res., 91, 10905-10936, 1986.

Li Q., D. J. Jacob, J. W. Munger, R. M. Yantosca, D. D. Parrish (2004), Export of NOy from the North American boundary layer: Reconciling aircraft observations and global model budgets, J. Geophys. Res., 109, D02313, doi:10.1029/2003JD004086.

Martin R. V., et al., An improved retrieval of tropospheric nitrogen dioxide from GOME, J. Geophys. Res., 107 (D20), 4437, doi:10.1029/2001JD001027, 2002.

Martin, R.V., C.E. Sioris, K. Chance, T.B. Ryerson, T.H. Bertram, P.J. Wooldridge, R.C. Cohen, J.A. Neuman, A. Swanson, and F.M. Flocke, Evaluation of space-based constraints on global nitrogen oxide emissions with regional aircraft measurements over and downwind of eastern North America, J. Geophys. Res., in press.

Muller, J. F., and G. Brasseur, IMAGES: A three dimensional chemical transport model of the global troposphere, J. Geophys. Res., 100, 16,445-16,490, 1995.

Olson, J.S. Carbon in live vegetation of major world ecosystems, ORNL-5862, Environmental Sciences Division Publication No. 1997, Oak Ridge National Laboratory, Oak Ridge, Tennessee, 1983.

Oppenheim, A. and R. Schafer, 1975: Digital Signal Processing. Prentice-Hall Inc, 585 pp.

Orlando, J. J., et al., Rate coefficient for the reaction of OH with CH2= C(CH3)C(O)OONO2 (MPAN), Atmos. Env., 36, 1895-1900, 2002.

Park R. J., D. J. Jacob, B. D. Field, R. M. Yantosca, M. Chin (2004), Natural and transboundary pollution influences on sulfate-nitrate-ammonium aerosols in the United States: Implications for policy, J. Geophys. Res., 109, D15204, doi:10.1029/2003JD004473

Parrish D. D., et al. (2004), Fraction and composition of NO y transported in air masses lofted from the North American continental boundary layer, J. Geophys. Res., 109, D09302, doi:10.1029/2003JD004226.

Pfister, G., P. G. Hess, L. K. Emmons, J.-F. Lamarque, C. Wiedinmyer, D. P. Edwards, G. Petron, J. C. Gille, and G. W. Sachse, Quantifying CO emissions from the 2004 Alaskan wildfires using MOPITT CO data, Geophys. Res. Lett., doi:10.1029/2005GL022995, 2005.

Pickering, K. E., Y. Wang, W.-K. Tao, C. Price, J.-F. Müller, Vertical distributions of lightning NO_x for use in regional and global chemical transport models, J. Geophys. Res., 103(D23), 31203-31216,,1998.

Pierce, R. B. et al., Regional Air Quality Modeling System (RAQMS) predictions of the tropospheric ozone budget over east Asia, J. Geophys. Res. 108, 8825, doi:10.1029/2002JD003176, 2003.

Price, C., J. Penner, M. Prather, NO_x from lightning 1. Global distribution based on lightning physics, J. Geophys. Res., 102(D5), 5929-5942, 10.1029/96JD03504, 1997.

Rault, D.F. Ozone profile retrieval from SAGE III limb scatter measurements, Journal of Geophysical Research, VOL. 110, D09309, doi:10.1029/2004JD004970, 2005

Rault, D.F., Taha, G., Validation of Ozone profiles retrieved from SAGE III limb scatter measurements, Journal of Geophysical Research, 2006JD007679, 2006, under review

Ravishankara A. R., E. J. Dunlea, M. A. Blitz, T. J. Dillon, D. E. Heard, M. J. Pilling, R. S. Strekowski, J. M. Nicovich, and P. H. Wine, *Redetermination of the rate coefficient for the reaction of O(1 D) with N 2*, Geophys. Res. Lett., 29 (15), doi:10.1029/2002GL014850, 2002.

Sander, S. P., R. R. Friedl, D. M. Golden, M. J. Kurylo, R. E. Huie, V. L. Orkin, A. R. Ravishankara, C. E. Kolb, M. J. Molina, *Chemical Kinetics and Photochemical Data for Use in Atmospheric Studies, Evaluation Number 14,* National Aeronautics and Space Administration, Jet Propulsion Laboratory, California Institute of Technology, Pasadena, 2003.

Savijarvi, H. 1995. Error growth in a large numerical forecast system. Mon. Wea. Rev. 123, 212-221

Schaack, T. K., T. H. Zapotocny, A. J. Lenzen and D. R. Johnson, 2004: Global climate simulation with the University of Wisconsin global hybrid isentropic coordinate model. J. Climate, 17, 2998-3016.

Schoeberl, M., R., Extratropical stratosphere-troposphere mass exchange, J. Geophys. Res, doi:10.1029/2004JD004525, 2004.

Singh, H. B., W. Brune, J. Crawford, D. Jacob, Overview of the Summer 2004 Intercontinential Chemical Transport Experiment-North America (INTEX-A), this issue.

Soja A.J., Cofer W.R., Shugart H.H., Sukhinin A.I., Stackhouse P.W. Jr., McRae D., and Conard S.G., 2004, Estimating fire emissions and disparities in boreal Siberia (1998 through 2002), *Journal of Geophysical Research*, doi:10.1029/2004JD004570.

Soja, A. J., J. Al-Saadi, R. B. Pierce, E. Alvarado, C. Kittaka, W. McMillian, G. Sachse, and J. j. Szykman, Description of a ground-based methodology for estimating boreal fire emissions for use in regional- and global-scale transport models, this issue.

Stajner, I., N. Winslow, R. B. Rood, S. Pawson , Monitoring of observation errors in the assimilation of satellite ozone data, *J. Geophys. Res.,* Vol. 109, No. D6, D06309 doi:10.1029/2003JD004118, 2004.

Stevenson, D. S., et al., Multimodel ensemble simulations of present-day and near-future tropospheric ozone., J. Geophys. Res., doi:10.1029/2005JD006338, 2006.

Stobie, J. M., et al., The use of optimum interpolation at AFGWC, Proc., 7th Conference on Numerical Weather Prediction, Montreal, Amer. Meteor. Soc., 43-49, 1985.,

Stobie, J. M., Algorithm Theoretical Basis Document for Statistical Digital Filter (SDF) Analysis System (Stretch-Grid Version), Data Assimilation Office, NASA Goddard Space Flight Center, Greenbelt, MD, 20771, 2000.

Stockwell, W.R., P. Middleton, J.S. Chang, and X. Tang, The second-generation regional acid deposition model chemiscal mechanism for regional air quality modeling, J. Geophys. Res., 95, 16343-16367, 1990.

Stockwell, W.R., F. Kirchner, and M. Kuhn, A new mechanism for regional atmospheric chemistry modeling, J. Geophys. Res., 102, 25847-25879, 1997.

Stolarski, R. S., S. L. Baughcan, W. H. Brune, A. R. Douglass, D. W. Fahey, R. R. Friedl, S. C. Liu, R. A. Plumb, L. R. Bole, H. Wesoky, and D. R. Worsnop, 1995 Scientific Assessment of the Atmospheric Effects of Stratospheric Aircraft, NASA Reference Publication 1381, 1995

Streets D. G., et al., An inventory of gaseous and primary aerosol emissions in Asia in the year 2000, J. Geophys. Res., 108 (D21), 8809, doi:10.1029/2002JD003093, 2003.

Talbot, R. H. Mao, B. Sive, Diurnal characteristics of surface level O3 and other important trace gases in New England, J. Geophys. Res., doi:10.1029/2004JD005449, 2005

Thompson A. M., et al., IONS-04 (INTEX Ozonesonde Network Study, 2004) New Perspective on Summertime UT/LS (Upper Troposphere/Lower Stratosphere) Ozone over Northeastern North America, submitted manuscript, 2006

Thompson A. M., et al., IONS-04 (INTEX Ozonesonde Network Study, 2004). 2. Tropospheric Ozone Budgets and Variability over Northeastern North America, this issue.

Vose, J.M., W.T. Swank, C.D. Geron, and A.E. Major (1996) Emissions from Forest Burning in the Southeastern United States: Application of a Model Determining Spatial and Temporal Fire Variation, in Biomass burning and global change, J.S. Levine, pp. 733-749, MIT Press, Cambridge, Mass.

Wayland, R. A. et al., Communicating real-time and forecasted air quality to the public, Environmental Management, 28-36, December 2002

World Meteorological Organization (WMO) (1993), Scientific assessment of ozone depletion: 1991, WMO Rep. 25, Geneva.

Wild, O., et al., Photochemical trajectory modeling studies of the North Atlantic region during August 1993, J. Geophys. Res., 101, 29,269-29,288, 1996.

Zapotocny, T. H., A. J. Lenzen, D. R. Johnson, F. M. Reames, and T. K. Schaack, A comparison of inert trace constituent transport between the University of Wisconsin isentropic-sigma model and the NCAR community climate model. Mon. Wea. Rev., 125, 120-142. 1997a.

Zapotocny, T. H., D. R. Johnson, T. K. Schaack, A. J. Lenzen, F. M. Reames, and P. A. Politowicz, Simulations of Joint Distributions of Equivalent Potential Temperature and an Inert Trace Constituent in the UW Isentropic- Sigma Model and CCM2. Geophys. Res. Let., 24, 865-868, 1997b.

Zapotocny, T. H., A. J. Lenzen, D. R. Johnson, F. M. Reames, P. A. Politowicz, and T. K. Schaack, Joint distributions of potential vorticity and inert trace constituent in CCM2 and UW isentropic-sigma model simulations. Geophys. Res. Let., 23, 2525-2528, 1996.

Zaveri, R.A. and L.K. Peters, A new lumped structure photochemical mechanism for large-scale applications, J. Geophys. Res., 104, 30387-30415, 1999.

Zinke, P.J., A.G. Strangenberger, W.M. Post, W.R. Emanuel, and J.S. Olson (1986) Worldwide Organic Soil Carbon and Nitrogen Data, NDP-018, 134 pp., Oak Ridge National Laboratory.

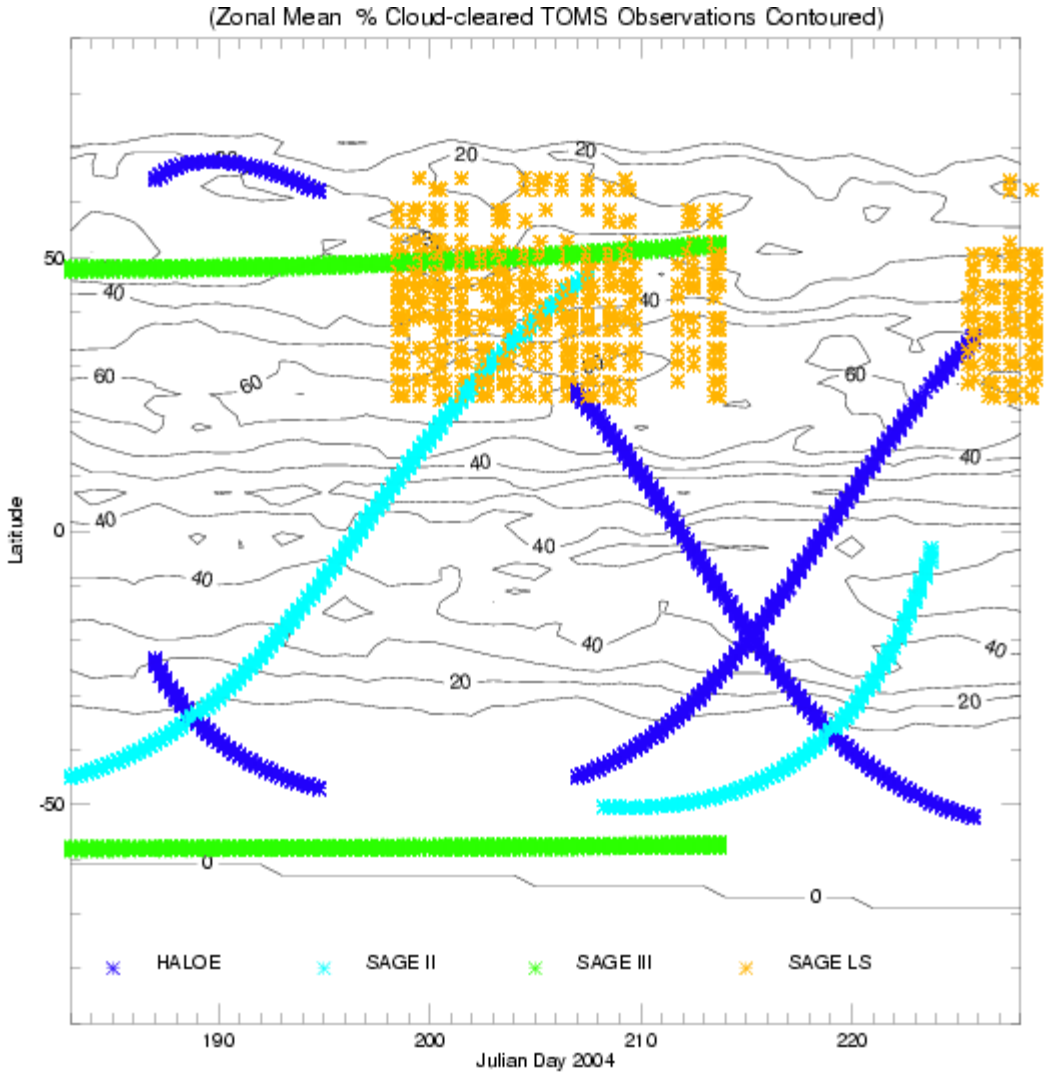

Figure 1: Latitude-time series of the frequency of observations used in the RAQMS assimilation. Symbols indicate the location of solar occultation and limb scattering observations. Contours indicate the density (zonal mean % of total) of cloud-cleared total column measurements.

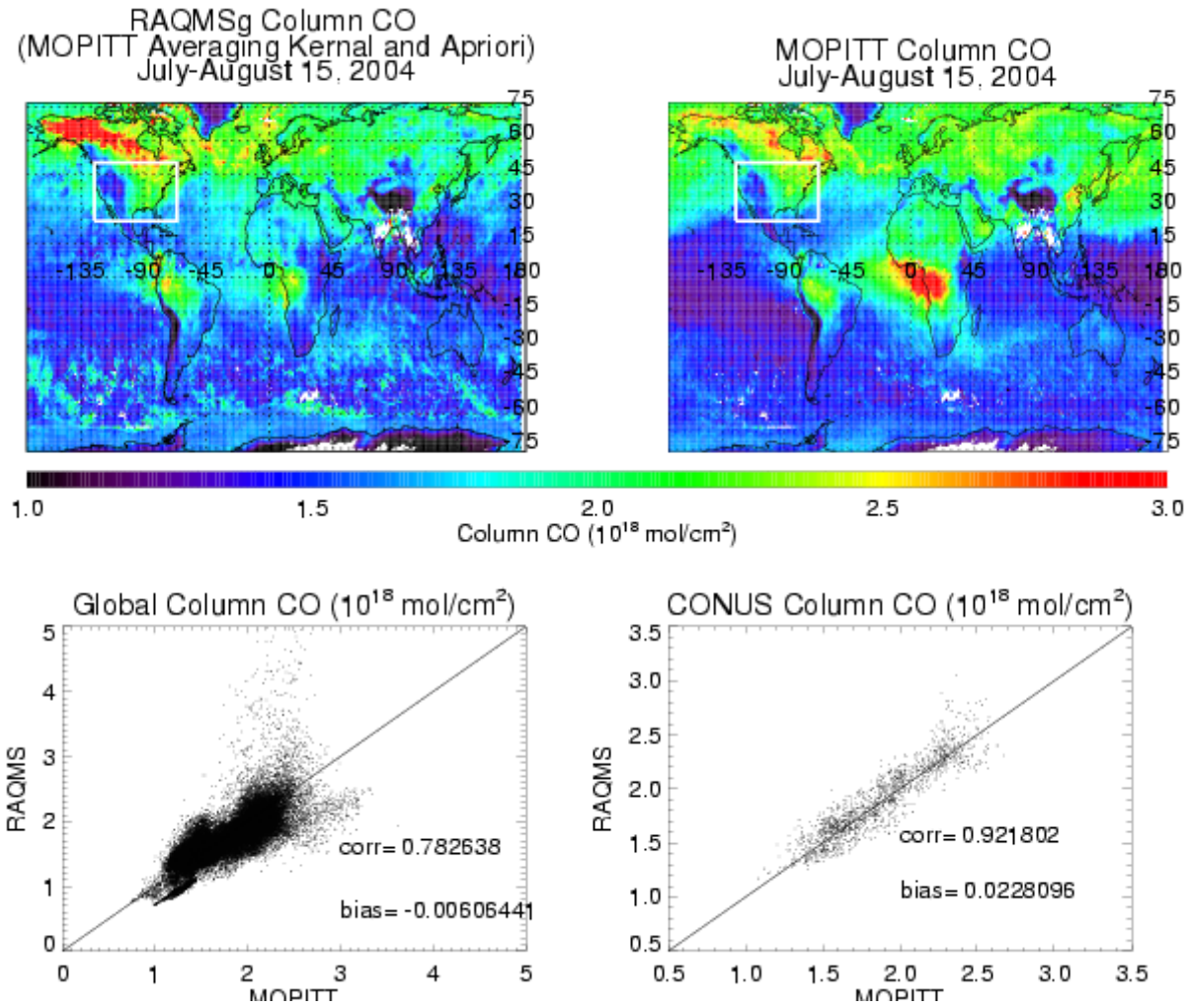

Figure 2: Comparison between RAQMS and cloud cleared MOPITT CO column (10^{18} mol/cm^2) for the period from July 01-August 15, 2004. Continental US budget domain is indicated in white.

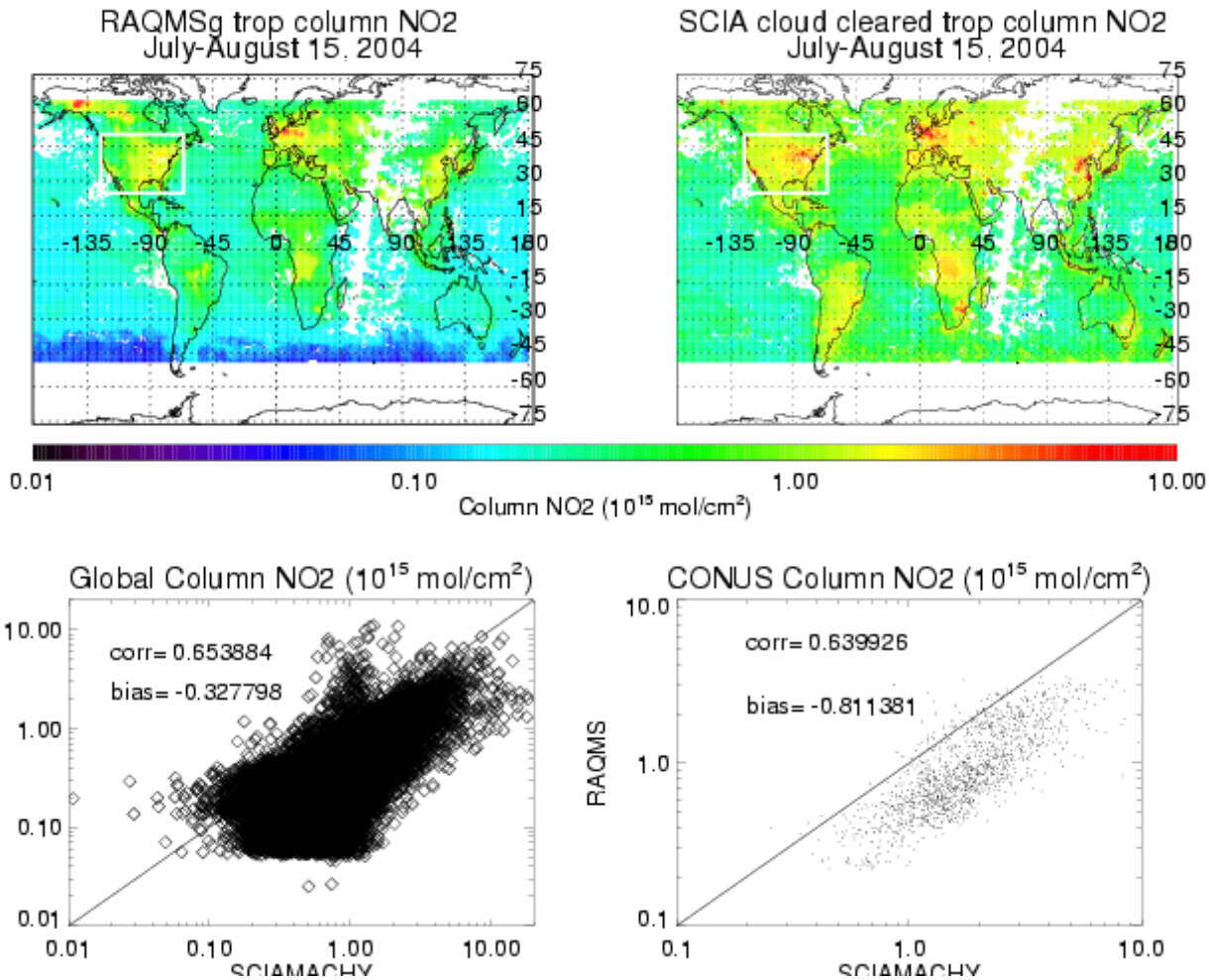

Figure 3: Comparison between RAQMS and cloud-cleared SCIAMACHY tropospheric NO2 column (10^{15} mol/cm^2) for the period from July 01-August 15, 2004. Continental US budget domain is indicated in white.

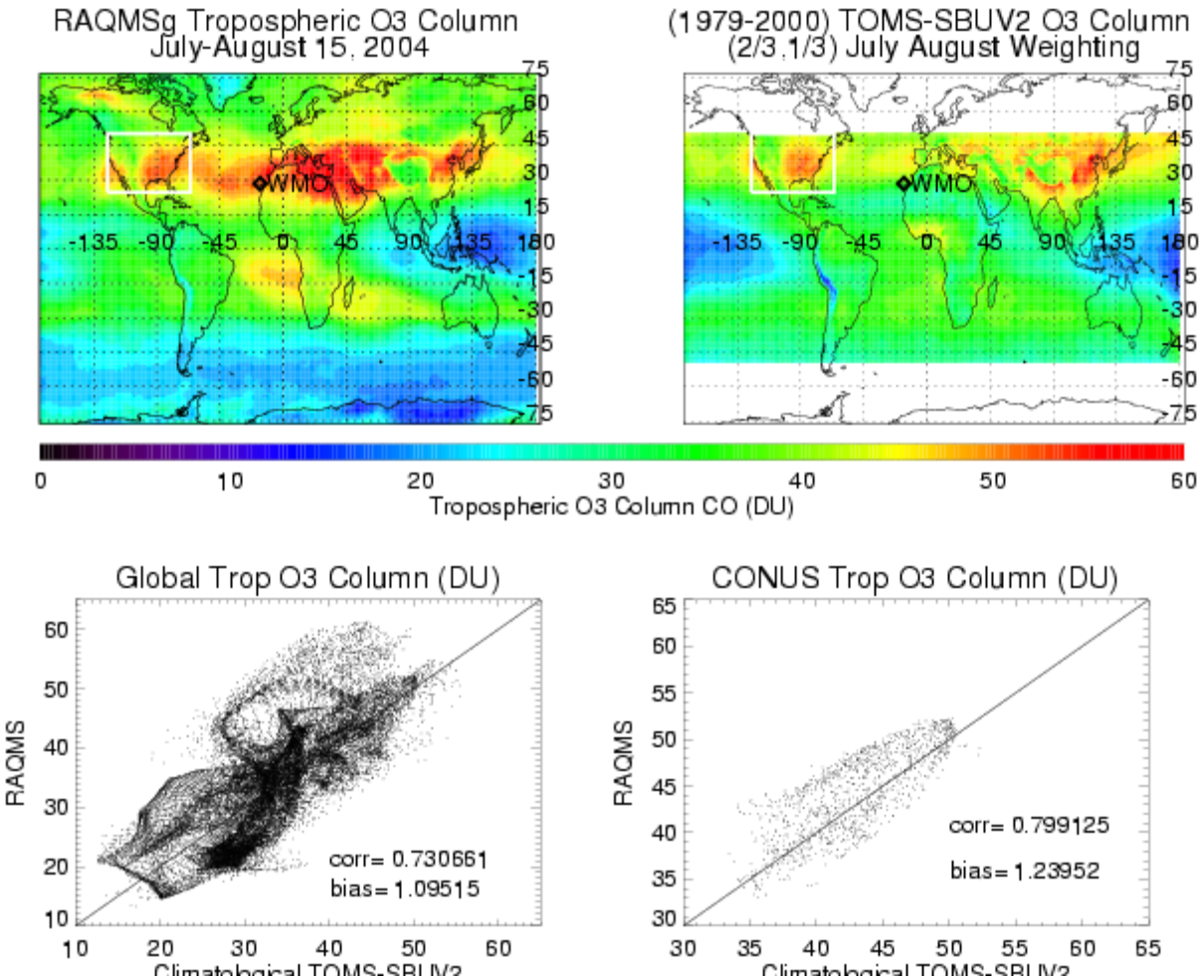

Figure 4: Comparison between RAQMS and climatological (1979-2000) tropospheric ozone column (DU) during the period from July 01- August 15, 2004. Continental US budget domain is indicated in white. The location of the WMO ozonesonde station at Santa Cruz, Tenerife is indicated by a diamond.

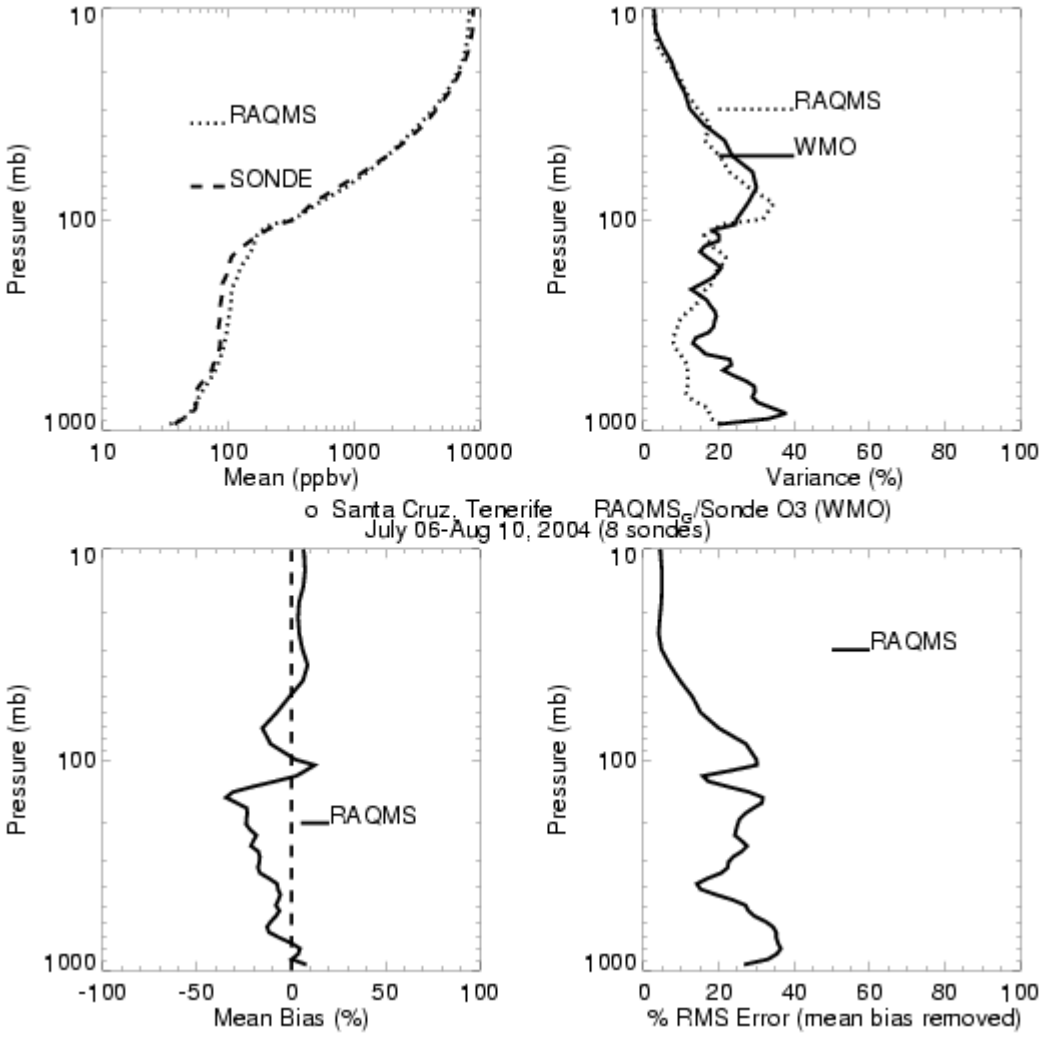

Figure 5: Comparison between RAQMS and Santa Cruz, Tenerife ozonesondes during July 06-August 10, 2004.

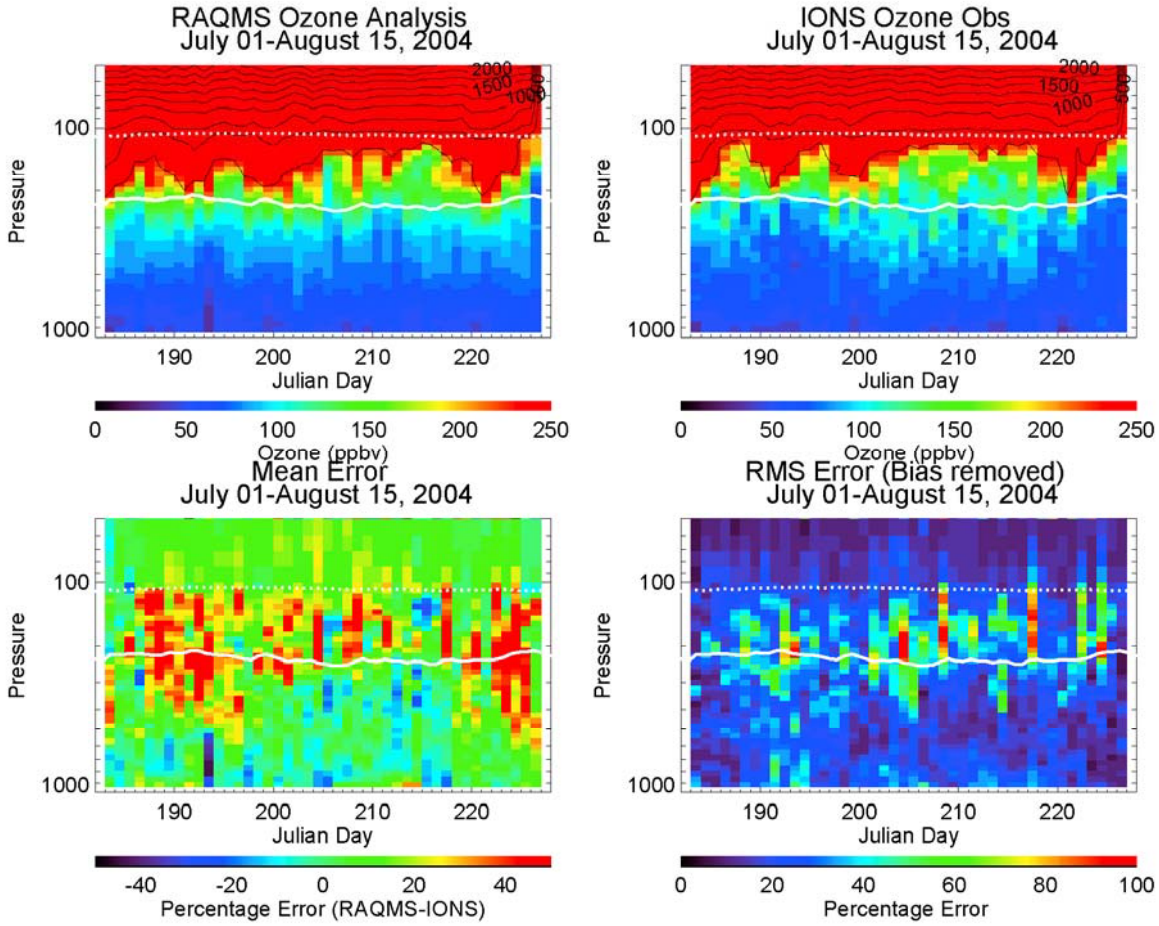

Figure 6: Composite timeseries of IONS ozonesonde data and coincident RAQMS ozone analyses (ppbv) during the period from July 01-August 15, 2004. Lower panels show composites of mean and RMS (mean Bias removed) errors (%).

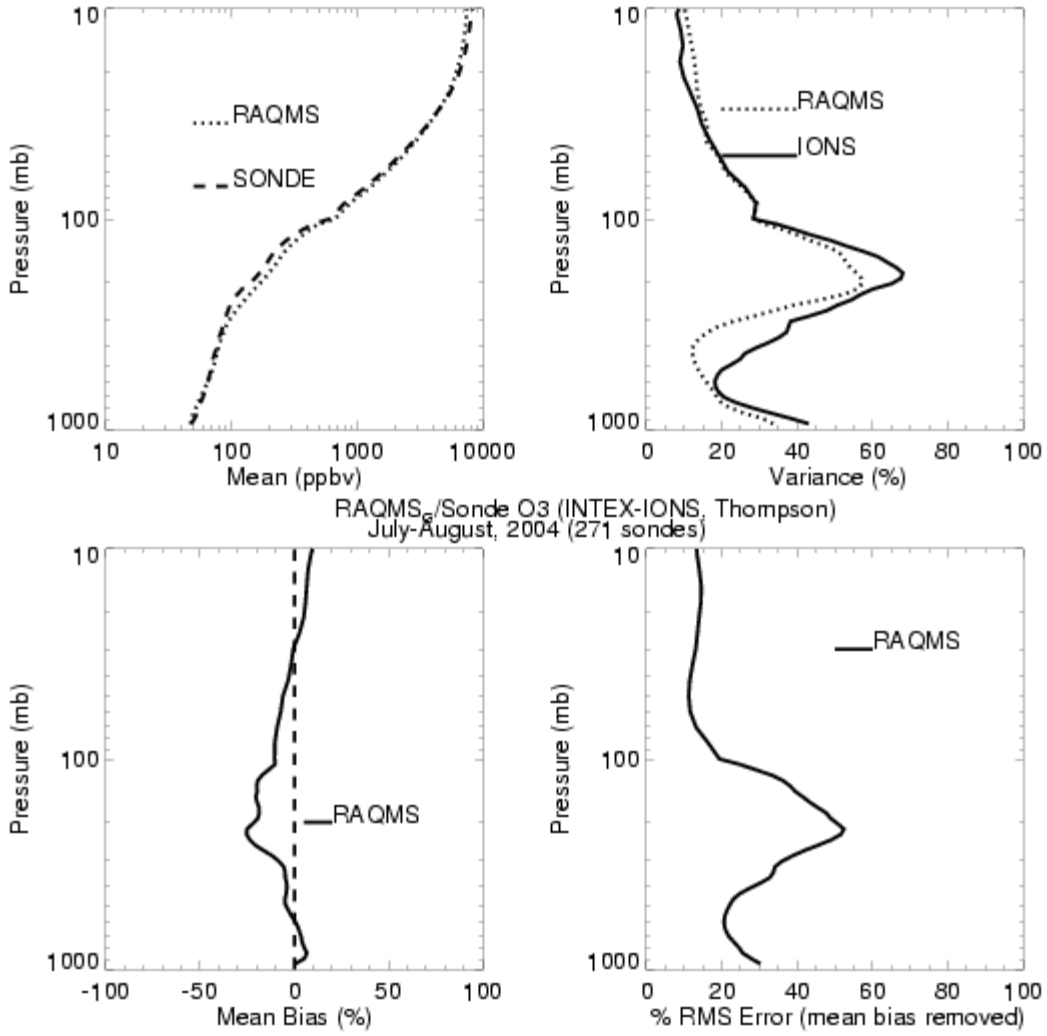

Figure 7: Comparison of time averaged IONS ozonesonde and coincident RAQMS ozone analyses during July 01-August 15, 2004.

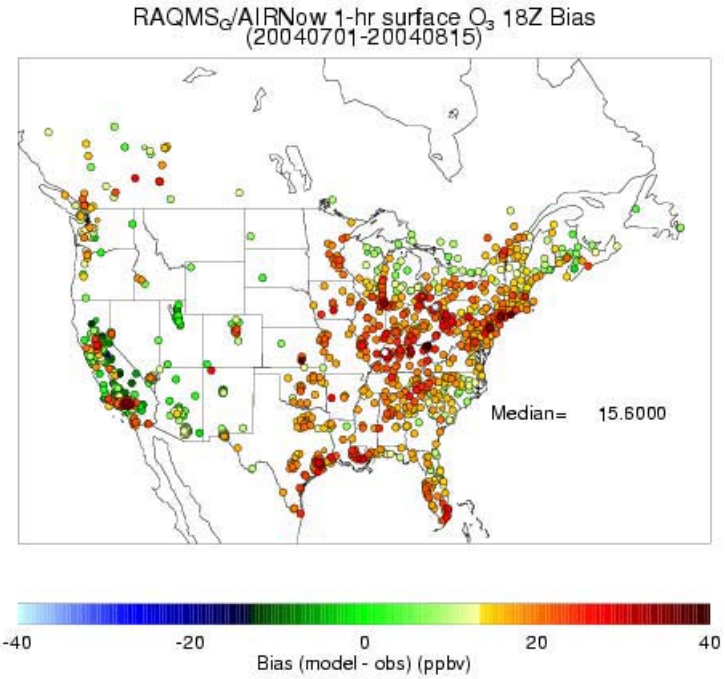

1

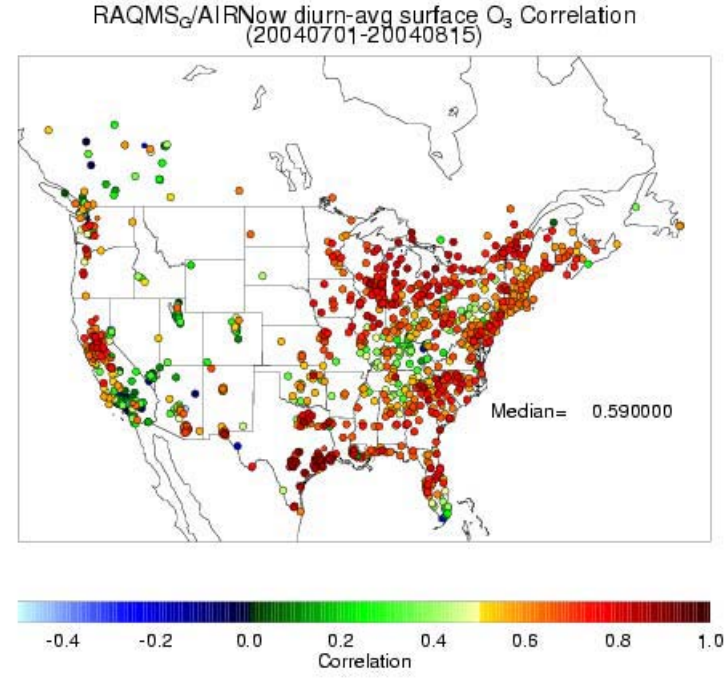

2
3

4 Figure 8: Comparisons between RAQMS and EPA AIRNOW surface ozone
5 measurements during July 01-August 15, 2004.

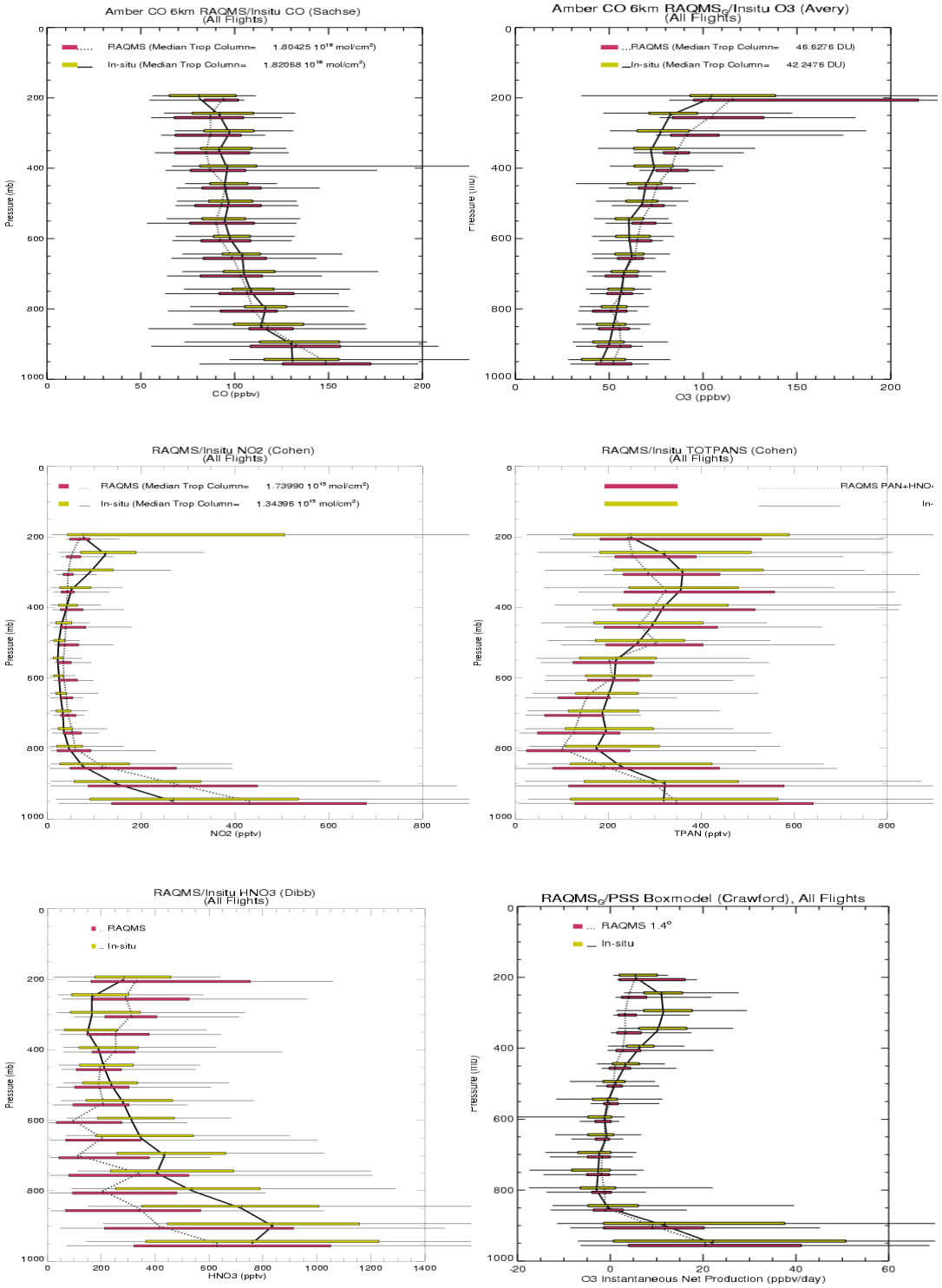

Figure 9: Comparisons between RAQMS and INTEX-A DC8 insitu observations of CO, O3 (upper panels), NO2, Total PANs (middle panels), HNO3, and observationally constrained boxmodel P-L calculations during July 01-August 15, 2004. CO and O3 are in ppbv, NO2, Total PANs, and HNO3 are in pptv, P-L is in ppbv/day.

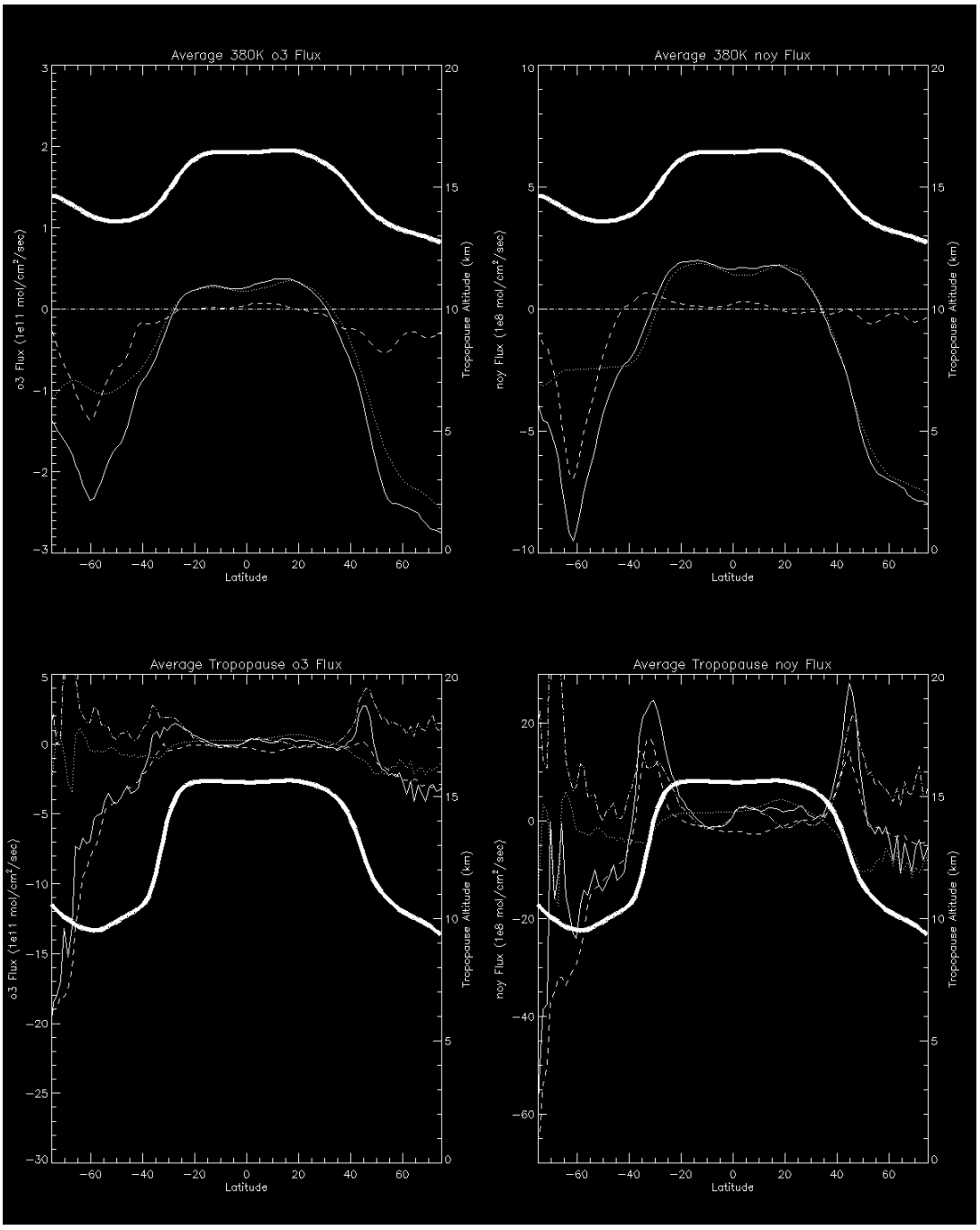

Figure 10: Zonally averaged global 380K (upper panels) and cross tropopause (lower panels) fluxes of O3 (10^{11} mol/cm^2/sec, left panels) and NOy (10^8 mol/cm^2/sec, right panels) during July 01-August 15, 2004. The thin solid line is the net flux, which is the sum of isentropic (dash-dot), diabatic (dotted), and movement of the surface (dashed). The bold line denotes the mean altitude (km) of the 380K and tropopause surface.

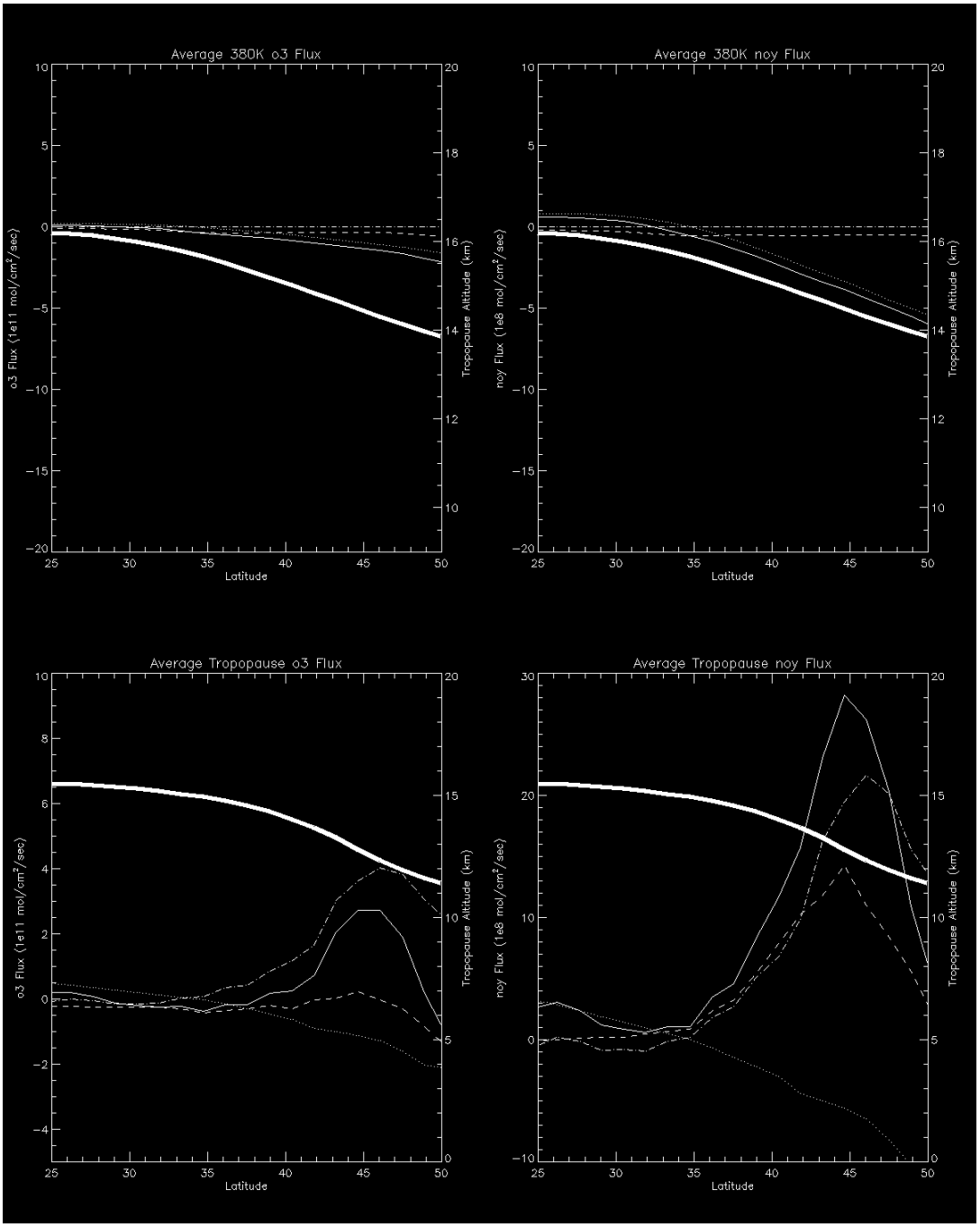

Figure 11: Zonally averaged Continental US 380K (upper panels) and cross tropopause (lower panels) fluxes of O3 (10^{11} mol/cm^2/sec, left panels) and NOy (10^8 mol/cm^2/sec, right panels) during July 01-August 15, 2004. The thin solid line is the net flux, which is the sum of isentropic (dash-dot), diabatic (dotted), and movement of the surface (dashed). The bold line denotes the mean altitude (km) of the 380K and tropopause surface.

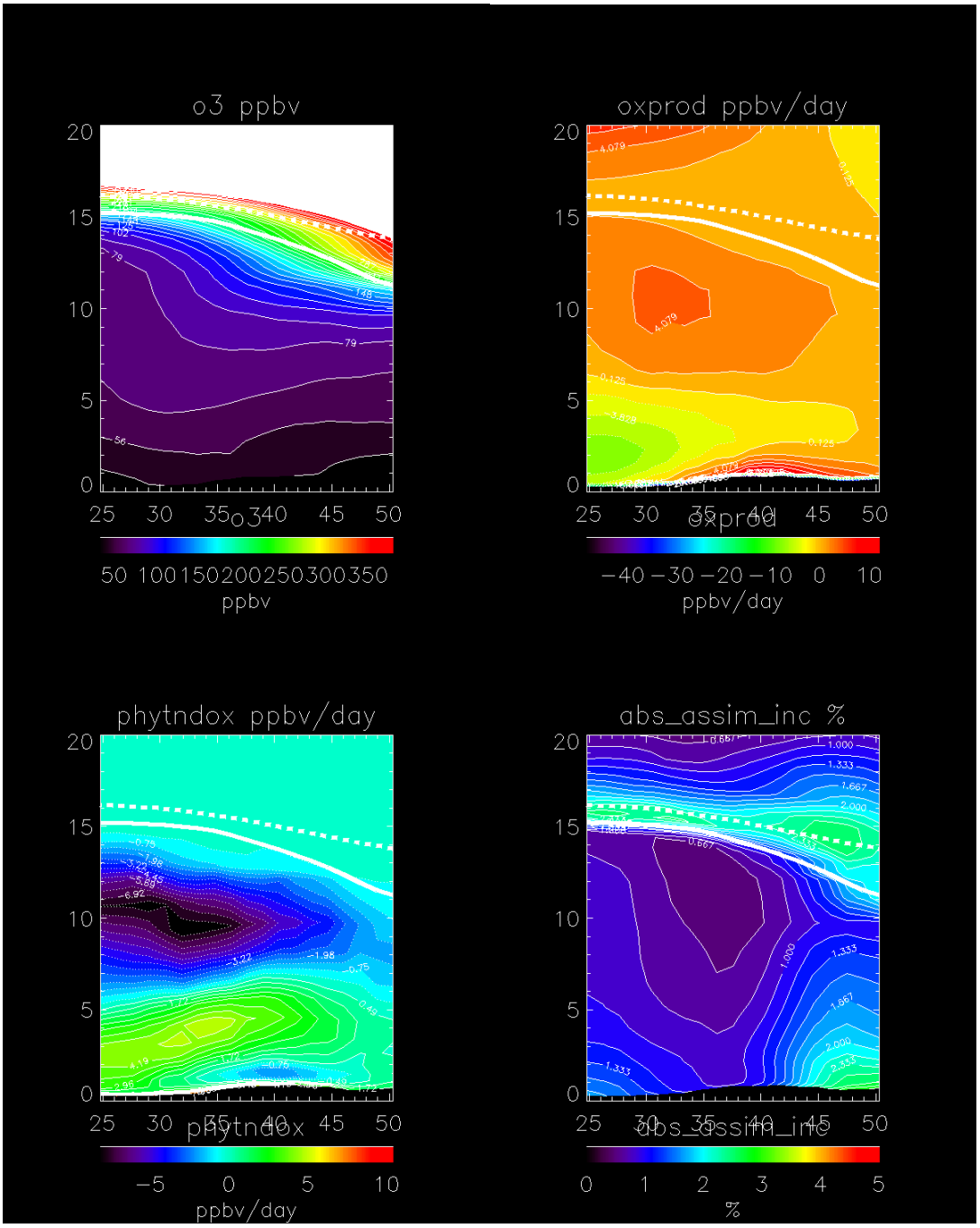

Figure 12: Time averaged zonal mean distribution of Continental US ozone (ppbv), Net P-L (ppbv/day), convective mixing tendencies (ppbv/day) and absolute assimilation increment (%) as a function of altitude (km) and latitude within the Continental US budget domain during July 01-August 15, 1004.

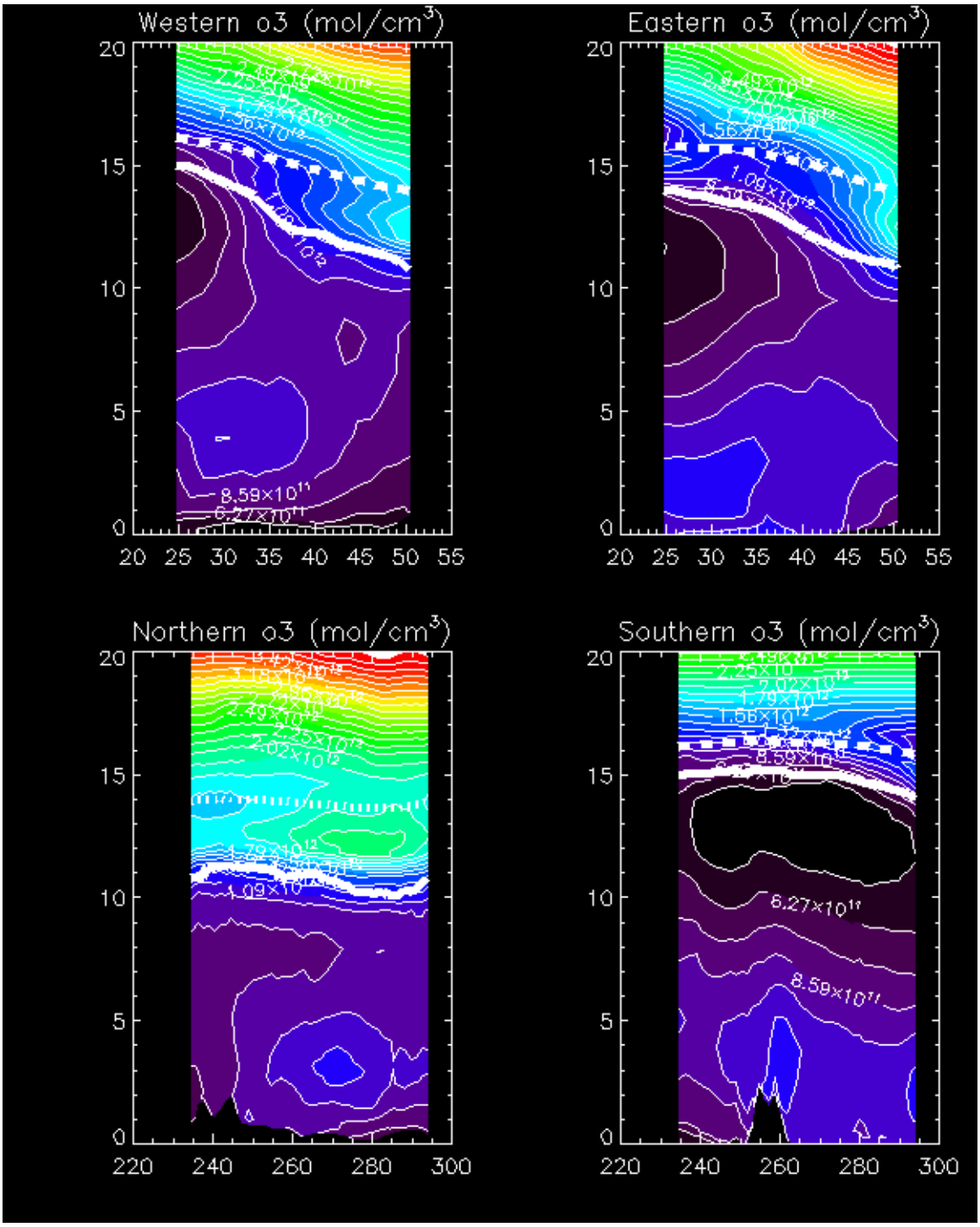

Figure 13: Time averaged ozone number densities (mol/cm3) for each of the lateral boundaries of the Continental US budget domain for July 01-August 15, 2004.

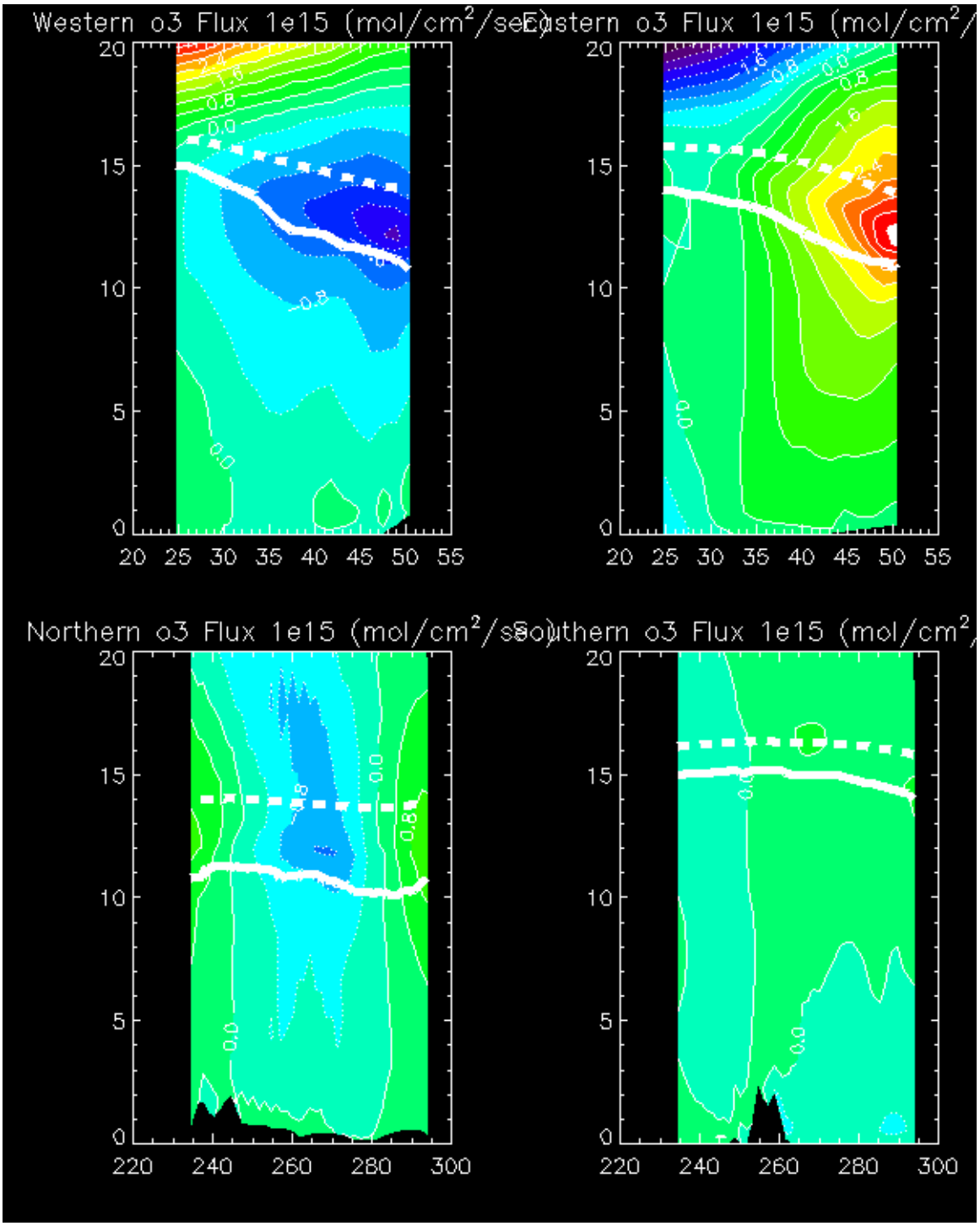

Figure 14: Time averaged ozone fluxes (mol/cm2/sec) for each of the lateral boundaries of the Continental US budget domain for July 01 – August 15, 2004. Negative fluxes are into the domain.

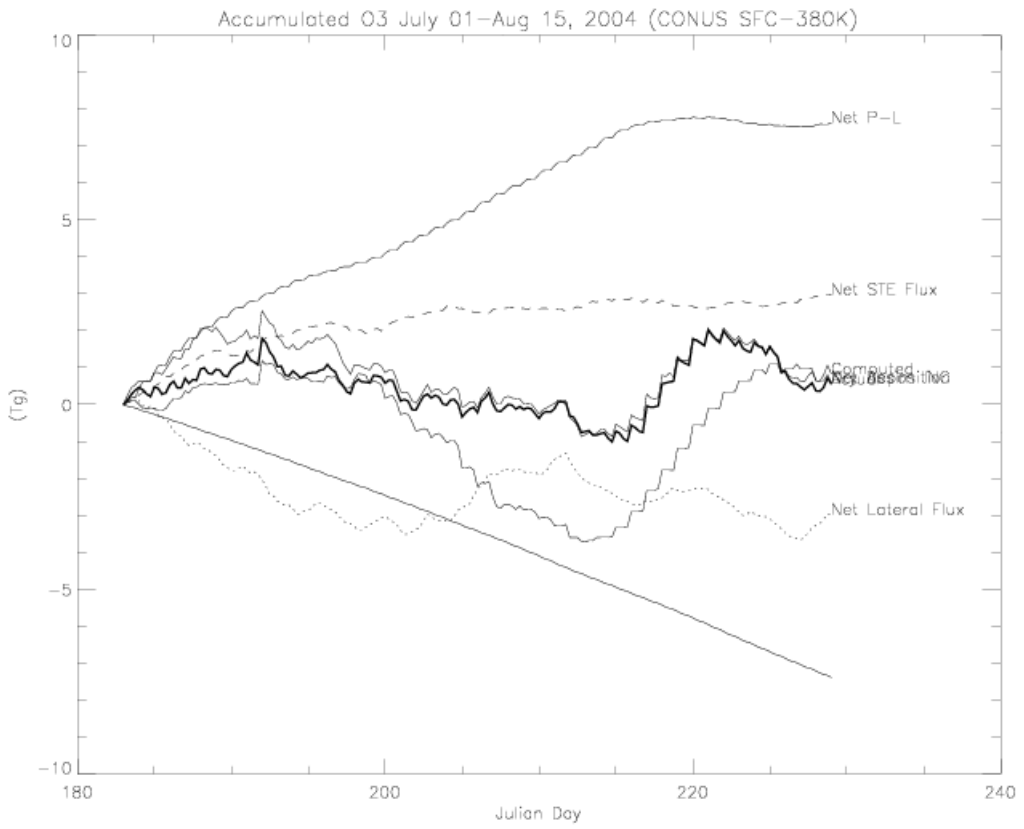

Figure 15: Time series of accumulated changes in Continental US ozone (Tg) for July 01 – August 15, 2004 due to P-L, 380K fluxes, lateral fluxes, ozone assimilation, and dry deposition. The actual and computed accumulation is also shown.

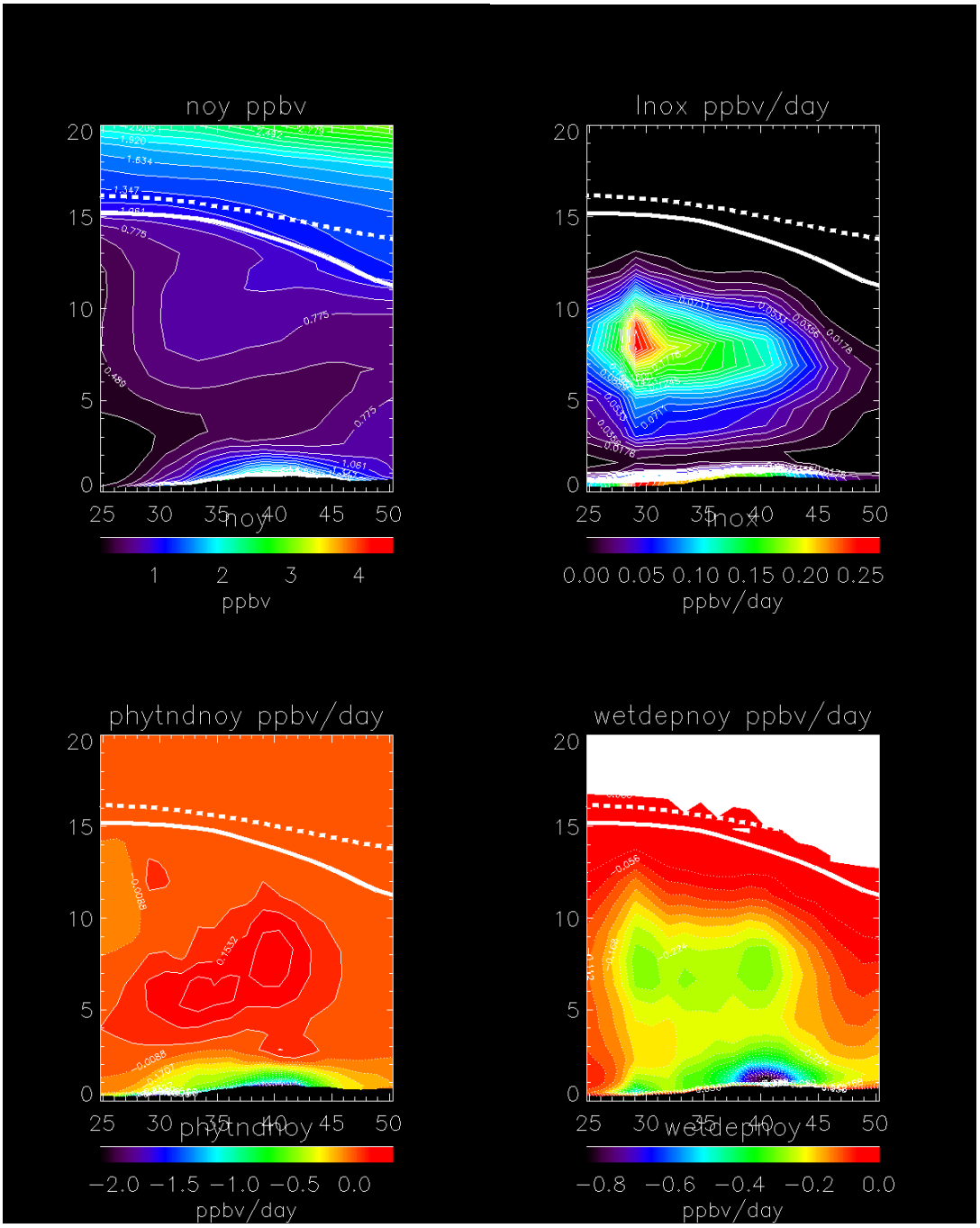

Figure 16: Time averaged zonal mean distribution of Continental US NOy (ppbv), Net production due to lightning NOx (ppbv/day), convective mixing tendencies (ppbv/day) and wet deposition (ppbv/day) as a function of altitude (km) and latitude within the Continental US budget domain during July 01-August 15, 1004.

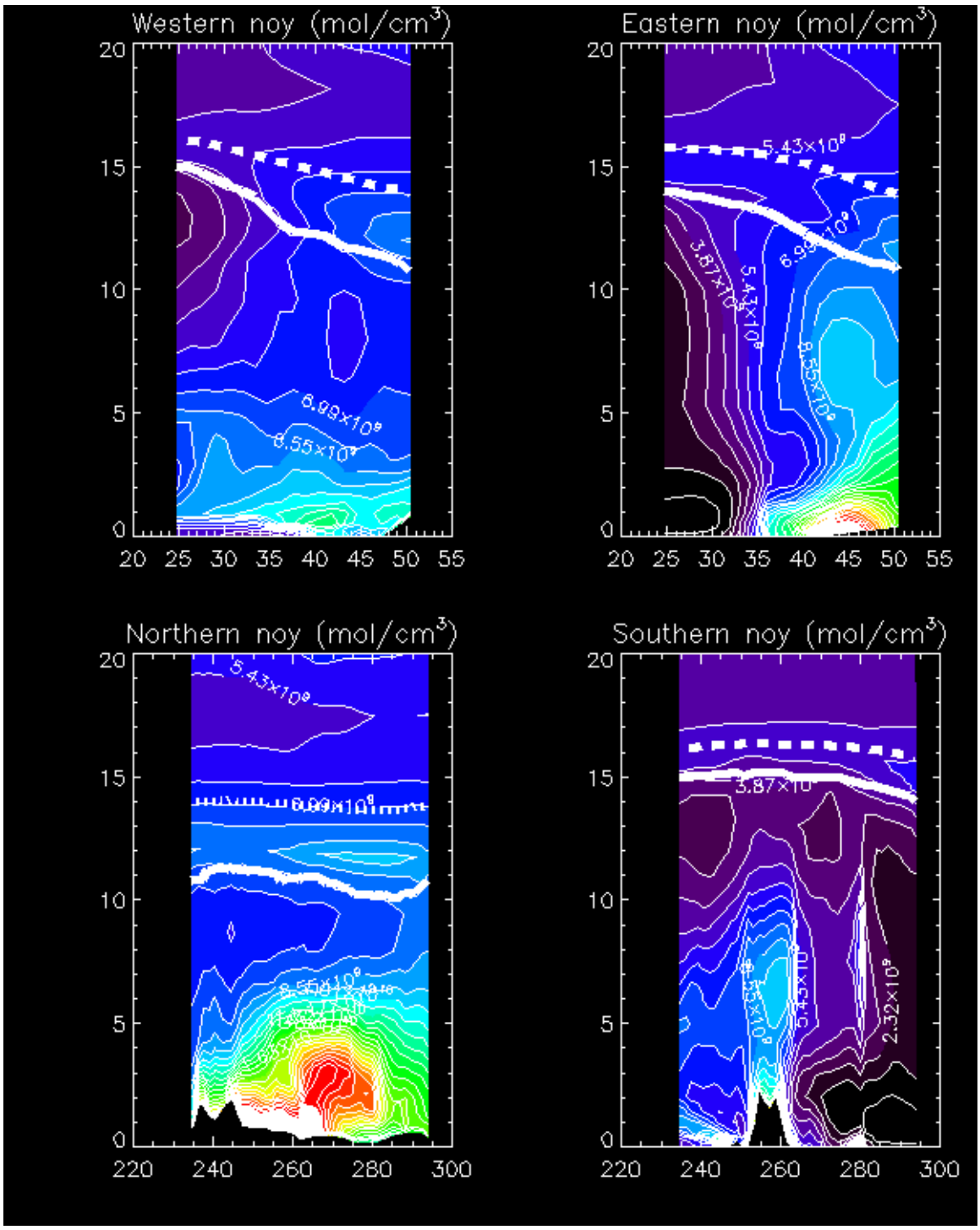

Figure 17: Time averaged NOy number densities (mol/cm3) for each of the lateral boundaries of the Continental US budget domain for July 01-August 15, 2004.

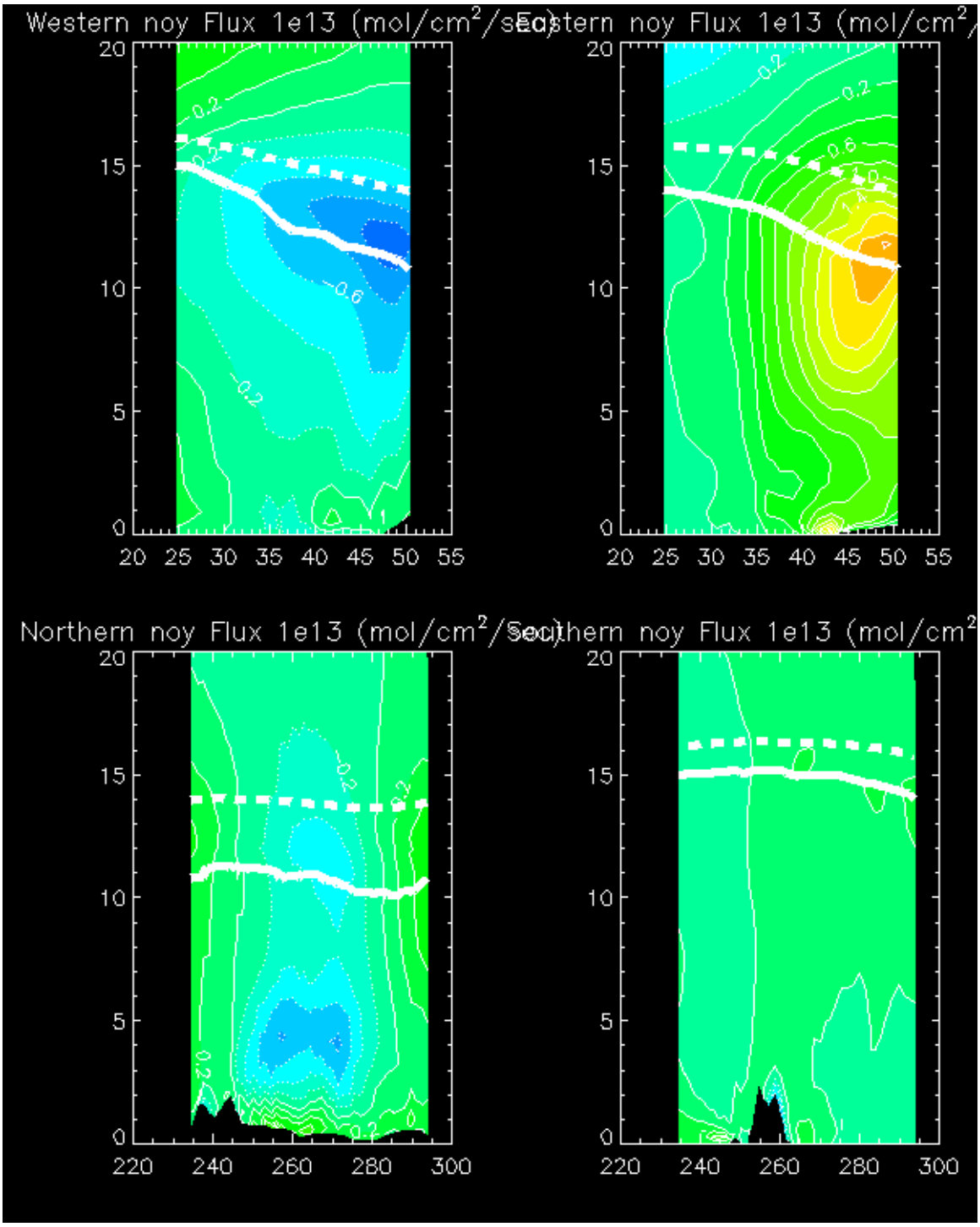

Figure 18: Time averaged ozone fluxes (mol/cm2/sec) for each of the lateral boundaries of the Continental US budget domain for July 01 – August 15, 2004. Negative fluxes are into the domain.

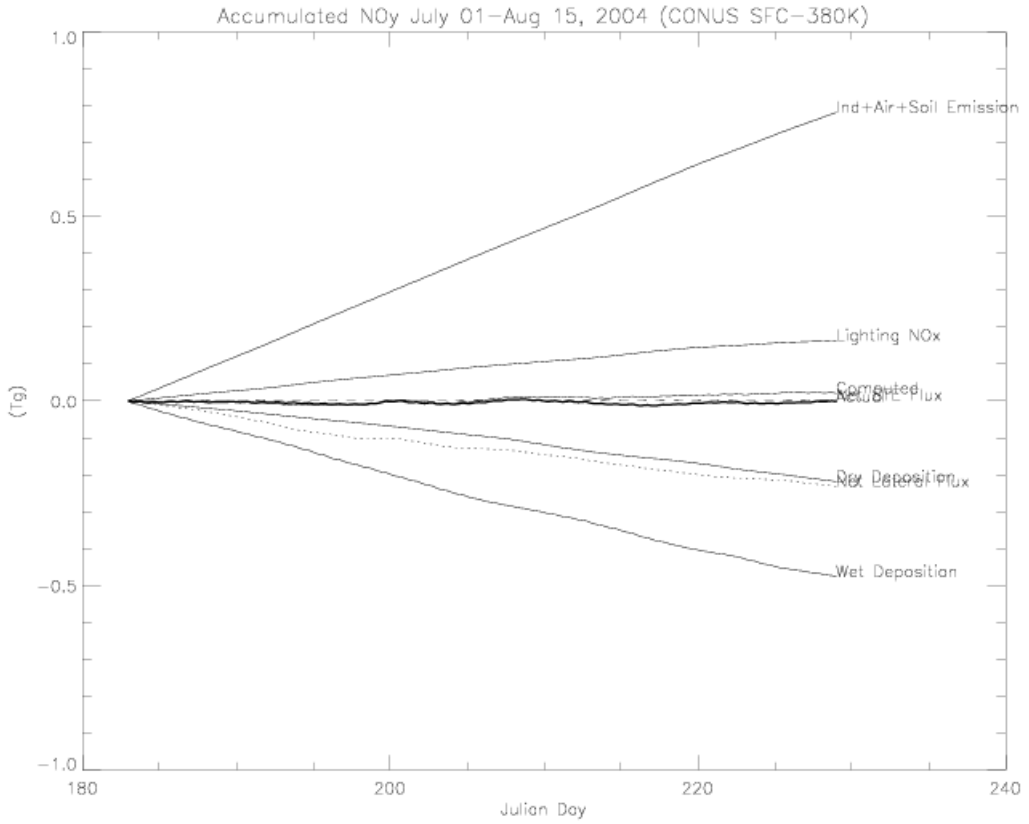

Figure 19: Time series of accumulated changes in Continental US NOy (Tg Nitrogen) for July 01 – August 15, 2004 due to emissions, 380K fluxes, lateral fluxes, lightning NOx, wet and dry deposition. The actual and computed accumulation is also shown.